Polyhedral boranes and carboranes as versatile species employed in the pursuit of imaging methods and of nanostructured materials

Sheila Michel

A thesis submitted to the Faculty of Graduate and Postdoctoral Studies
in partial fulfillment of the requirements for the degree of Master of Science
in the Ottawa-Carleton Chemistry Institute

Department of Chemistry, University of Ottawa

Université d'Ottawa
University of Ottawa

Candidate

_____
Sheila Michel

Supervisor

_____
Professor D. S. Richeson

Table of Contents

Acknowledgements iii

List of Figures iv

List of Schemes vii

List of Tables viii

List of Abbreviations ix

Abstract 1

Chapter 1: Introduction 3

Polyhedral boranes, Organic-Inorganic Block Copolymers, and Self-Assembly 3

Chapter 1.2: Material Characterization for Block Copolymers 15

Chapter 2: Carborane Raman Reporters 21

Introduction 21

Results and Discussion 32

Experimental 35

Chapter 3: Organic- Organodecaborane block copolymers 40

Introduction 40

Results and Discussion 48

Experimental 66

Chapter 4: Boron Nitride and Boron Carbonitride Ceramics 76

Introduction 76

Results and Discussion 81

Experimental 88

Conclusion and Future Directions 89

Appendix 90

References 93

Acknowledgements

First, I would like to express my deepest gratitude to my supervisor, Dr. Darrin Richeson, for his support and guidance during my tenure as a Master's student. I would also like to thank Dr. Patrick Malenfant for his advice with my research project, and give special thanks to Dr. Yun Liu, Dr. Sadok Letaif, and Rola Mansa for their services and assistance on the analysis equipments at the CCRI centre.

I would like to thank my group members; Titel Jurca, Ahmed Farghal, Sarah Ouanounou, and Nastaran Ghorbanianfarahabadi for their help and putting up with me and my weirdness.

Lastly, I would like to thank my family, my mom Beatrice Pointejour and my sister Ashley Michel for their financial and emotional support. I would like to thank my friends; Asma Inam, Sharifa Lambert, Niveen Eldin, Elena Dimitrijevic and Kensly Guerrier for their support.

List of Figures

Figure 1.1 - Decaborane numbering system of the boron atoms……..……6

Figure 1.2[1] **–** Diagram of *closo, nido,* and *arachno* boranes (hydrogen atoms other than the BH framework are omitted……..……7

Figure 1.3 – Structures of the *ortho*-carborane (**1**), *meta*-carborane (**2**), and *para*-carborane (**3**). The numbers represents the position of each vertex of these icosahedra carboranes……..9

Figure 1.4 [2] - Schematic of various ways to functionalize an inorganic building block as a precursor from polymerization forming various forms of hybrid polymers……..11

Figure 1.5 [3] -Theoretical phase diagram for linear AB diblock copolymers. (Upper) Four morphologies can be predicted: spherical (S), cylindrical (C), gyroid (G), and lamellar (L). (Lower) microdomain structures of f_A as it increases with fixed $\chi_{AB}N$ of a diblock copolymer……..15

Figure 1.6[4]- Diffraction pattern from X-ray powdered diffraction (XRD) where θ represents the angle of incidence of the X-ray and d represents the spacing between the atom layers……20

Figure 2.1[5] -The three types of scattering by a molecule excited by a incident light beam. Rayleigh scattering the molecules excited returns back to its original state. Stokes and Anti-stokes scattering differ in energy by ΔE……22

Figure 2.2[6] - Diagram of the silver NP with *ortho*-carborane thiol, thiolated secondary antibody, and thiolated polyethylene glycol (PEG)chains ……..26

Figure 2.3[7]-Boron neutron capture nuclear reaction between ^{10}B and thermal neutrons with the release or ^{7}Lithium and alpha particles……27

Figure 2.4- Current leading BNCT agents **(1)** sulfhydryl borane $Na_2B_{12}H_{11}SH$ (BSH) and **(2)** p-dihydroxyborylphenylalanine (BPA)……29

Figure 3.1- Three different generations of Grubbs catalysts. First generation of Grubbs (1), Second generation of Grubbs (2), and Third generation of Grubbs (3)……41

Figure 3.2 – Comparison ^{1}H NMR of $p(NBE)_{60}$-$p(NDB)_{40}$ block copolymer and the homopolymers of p(NBE) and p(NDB) . The peaks boxed in red represent the peaks exclusive to the p(NDB) block in the block copolymer product. The peaks boxed in black represent the peaks exclusive to the p(NBE) block in the block copolymer product……..54

Figure 3.3- TGA/DTA analysis of p(NDC)-*b*-p(NDB). From RT to 400^{o}C a ramp of 10^{o}C/min was applied and dwelled for 20 mins continued at a ramp of 10^{o}C/min to 1000 ^{o}C……59

Figure 3.4- DSC analysis of the block copolymers. DSC curves at ramp of 10^{o}C/min from RT to 550^{o}C for (A) p(NBE)$_{70}$-*b*-p(NDB)$_{30}$, (B) p(NBE)$_{60}$-*b*-p(NDB)$_{40}$, (C) p(NDC)$_{30}$-*b*-p(NDB)$_{70}$, and (D) p(NDC)$_{40}$-*b*-p(NDB)$_{60}$ .Different ramp cycle for (E) p(NDC)$_{70}$-*b*-p(NDB)$_{30}$ and (F) p(NBE)$_{50}$-*b*-p(NDB)$_{50}$ that have undergone second heating starting at RT to 150^{o}C at 2^{o}C/min followed by a ramp of 5^{o}C/min to 550^{o}C……..62

Figure 3.5- SEM images block copolymers after evaporation. (A) p(NBE)$_{50}$-*b*-p(NDB)$_{50}$ after evaporation in toluene; (B) p(NBE)$_{50}$-*b*-p(NDB)$_{50}$ after evaporation in DCM; (C) p(NBE)$_{50}$-*b*-p(NDB)$_{50}$ after evaporation in chloroform; (D) p(NDC)$_{70}$-*b*-p(NDB)$_{30}$ after evaporation in chloroform; (E) p(NBE)$_{60}$-*b*-p(NDB)$_{40}$ after evaporation in chloroform; (F) p(NBE)$_{60}$-*b*-p(NDB)$_{40}$ after evaporation in THF……..64

Figure 3.6 [8]-TEM images on p(NBE)$_{70}$-*b*-p(NDB)$_{30}$ after slow solvent evaporation in THF (A) and in Chloroform (B)……..65

Figure 4.1 [9]- Diagrams of the most stable forms of BN. (A) α-BN or hexagonal-BN, (B) β-BN or cubic-BN……..77

Figure 4.2- EDS of the BN ceramic from p(NBE)$_{60}$-*b*-p(NDB)$_{40}$ polymer pyrolyzed under ammonia gas at 1000^{o}C. Boron (38.84%), nitrogen (38.39%), and oxygen (22.77%) were detected……..82

Figure 4.3- EDS of the BCN ceramic from p(NBE)$_{60}$-*b*-p(NDB)$_{40}$ polymer pyrolyzed under nitrogen gas at 1000^{o}C. Carbon (51.17%), boron (11.06%), nitrogen (11.34%), and oxygen (12.12%) were detected……..84

Figure 4.4- SEM images of p(NBE)$_{60}$-p(NDB)$_{40}$ polymer evaporated from chloroform than pyrolyzed under ammonia gas creating lamellar morphology patterns……..86

Figure 4.5- SEM images of $p(NBE)_{60}$-$p(NDB)_{40}$ polymer evaporated from THF than pyrolyzed under nitrogen gas……87

List of Schemes

Scheme 2.1- Reaction scheme of the synthesis of 1,12- bis(mercapto) -*p*-carborane follow by the synthesis with 3-bromopropionitrile to produce 1-(1-thiopropionitrile)-12-mercapto-*p*-carborane……33

Scheme 3.1- Catalytic process of the activation of Grubbs 3 and its intermediate species…..43

Scheme 3.2- Reaction Scheme of hydroboration of decaborane and norbornadiene catalyzed by 3% mol of titanocene dicarbonyl……45

Scheme 3.3- Catalytic process of titanocene dicarbonyl catalyst during hydroboration of decaborane and norbornadiene……..47

Scheme 3.4- Schematic of the 2-step diblock polymer synthesis. P(norbornene) was first synthesize than without termination of Grubbs 3, a mixture of both norbornenyl-decaborane isomers were added and quenched with ethyl vinyl ether……51

Scheme 3.5- Schematic of the 2-step diblock polymer synthesis. P-(dimethyl cis-5- norbornene-endo-2,3- dicarboxylate) was first synthesize than without termination of Grubbs 3, a mixture of both norbornenyl-decaborane isomers were added and quenched with ethyl vinyl ether……..56

Scheme 4.1[10]- Schematic of poly(vinylpentaborane) pyrolyzed to 350^{o}C under a ammonia gas to create a borazanaphthalene intermediate before producing BN……79

List of Tables

Table 1.1- The relationship between the borane structure, its molecular formula and the skeletal electron pair using Wade's rule. The general structure of the borane is defined by the skeletal electron pair and its formula……5

Table 3.1- Various compositions of the diblock polymer synthesized with Grubbs 3 under various temperatures……50

Table 3.2- A concentrated list of the p(NBE)-b-p(NDB) diblock copolymers that were further analyzed showing the actual monomer composition in the polymer and its yields……52

Table 3.3- A concentrated list of the p(NDC)-b-p(NDB) diblock copolymers that were further analyzed showing the actual monomer composition in the polymer and its yields……57

List of Abbreviations

BNCT	Boron neutron capture therapy
BPA	*p*-dihydroxyboryl-phenylalanine
BSH	Sulfhydryl borane
DCM	Dichloromethane
DMF	Dimethylformamide
DMSO	Dimethyl sulfoxide
DP	Degree of polymerization
DRI	Differential refractometry index
DSC	Differential scanning calorimetry
DTA	Differential thermal analysis
EA	Elemental analysis
EDS	Energy-dispersive x-ray spectroscopy
EGFR	*Epidermal growth factor receptor*
LALLS	Low angle laser light scattering
MALLS	Multi –angle laser light scattering
MS	Mass spectrometer
Mn	Number average molecular weight
Mw	Weight average molecular weight
NBE	Norbornene
NDB	6-(5-norbornenyl)-decaborane
NDC	Dimethyl cis-5- norbornene-endo-2,3-dicarboxylate
NMR	Nuclear magnetic resonance
PCy_3	Tricyclohexylphosphine
PDI	polydispersity index
RI	Refractive Index

ROMP	Ring-opening metathesis polymerization
RT	Room temperature
SEM	Scanning electron microscopy
SERS	Surface-enhanced Raman scattering
TEM	Transmission electron microscopy
T_g	Glass transition temperature
TGA	Thermal gravimetric analysis
T_m	Melting temperature
UV/VIS	Ultraviolet-visible spectroscopy

Abstract

Polyhedral boranes and carboranes have acquired their popularity for constructing meso and nano-size structures for an array of applications from pharmaceuticals to material science. These three-dimensional boranes range from 4 to 22 boron atom per molecules with delocalized bonding analogous to aromatic compounds.

The unique vibrational spectroscopy of the BH function allows for possible application of these species to bioimaging. Silver nanoparticles functionalized with *ortho*-carboranes have been reported for bioimaging using Surface-enhanced Raman scattering (SERS). The silver nanoparticles were functionalized with antibodies specific to cancer cell receptors. Bonding thiol-substituted carboranes to these particles allowed for observation of enhanced Raman signals as the imaging mode. Here, attempts to synthesize second generation carborane molecules with additional Raman-active group such as nitrile were conducted.

Hybrid diblock copolymers have the ability to self-assemble in different morphological patterns depending on the type and ratio of monomers and the compatibilities in various solvents. Linear hybrid diblock copolymers were synthesized by ring-opening metathesis polymerization (ROMP) reactions with norbornenyl-based decaborane and various amounts of norbornene and norbornenyl-ester derivative monomers. Their self-assembly behaviour in various solvents were characterized by NMR, TGA, DSC, and SEM. P(norbornene)$_{60}$-*b*-p(norbornenyl-decaborane)$_{40}$ polymers showed lamellar morphology patterns when slowly evaporated from chloroform. Based on results and the SEM images, a few of these diblock copolymers were used

as ceramic precursors and pyrolyzed to elevated temperatures forming boron nitride and boron carbonitride nano-ordered ceramics.

Chapter 1: Introduction

Template-assisted self-assembly is a method of choice for producing morphological knitting patterns of block copolymers. The main disadvantages to this method includes; the cost of the equipment/template itself, the multiple steps needed to complete the self-assembly, and the stringent properties needed for the required interaction between and the template and BCP.[11] Non-templated self-assembly is a relatively inexpensive alternative route to achieve tailored nanoscale patterns of polymeric mixtures and the morphologies can be controlled by changing the monomers' volume fraction, functional groups, the length homopolymers segments .[8] Here, we investigated self-assembly of block copolymers with polyhedral borane moieties.

Polyhedral boranes, Organic-Inorganic Block Copolymers, and Self-Assembly

Diborane (B_2H_6), the simplest borohydride, has 12 valence electrons with eight electrons of those being regular 2-centre 2-electron (2c-2e) bonds and the remaining four being involved in bonding in bridges. The bridges bonding involves three atoms sharing two electrons formally known as 3-center 2-electron (3c-2e) bonding of B-H-B with the boron centre being pseudo-tetrahedral.[12] Similar to most boranes, diborane reacts spontaneously with air and is flammable producing a green flame. Polyhedral boranes are comprised of series of triangular coordinated boron hydrides, also known as deltahedra, acquiring geometric shapes from tetrahedron to icosahedron.[1] With larger borane clusters, the molecules contain B-B-B 3c-2e bonds in addition to the B-H-B 3c-2e bonds seen in diboranes.[12] These three-dimensional

boron clusters have been synthesized for several decades for applications ranging from biomedical to materials science nanotechnology.[13]

When describing the structure and bonding of boranes, Wade's rule is applied to rationalize and determine the shape of the cluster by calculating the total number of skeletal electron pairs available for bonding.[1] This is analogous to Hückel's rule for aromaticity in hydrocarbon where $(4n + 2)$ π electrons corresponds to an aromatic system such as benzene and naphthalene.[14] The classification system is based on the deltahedral *closo* structure $B_nH_n^{2-}$ (n= 5-12). [14] The deltahedral borane structures with all the vertices intact having a closed framework are called *closo* structures. Additional sub-classifications include: *nido*-borane, with one missing vertex resembling a birds' nest; *arachno*-boranes, which has two missing vertices with similar appearance to spider web; and *hypho*-boranes, with a net–like structure (Figure 1.1).[15] Wade recognized that there is a relation between the structural relationship and the number of valence electrons associated with the skeletal bonding of these borane molecules.[16] A $(n+1)$ rule is used to determine the electron pairs necessary for the skeletal bonds in the structure where n represents the number of boron atoms (or number of vertices) (Table 1.1).[15] For example, $B_6H_6^{-2}$, there are 26 valence electrons with a total of 13 electron pairs. To calculate the skeletal electron pairs (SEP), subtract 6 electron pairs belonging to BH to have 7 electron pairs remaining for B-B and B-B-B bonds. Since n=6 (boron vertices) and n+1=7, the structure of the borane is *closo*.

Table 1.1- The relationship between the borane structure, its molecular formula and the skeletal electron pair using Wade's rule. The general structure of the borane is defined by the skeletal electron pair and its formula.

Structure	Formula	Skeletal electron pairs
closo	$[B_nH_n]^{2-}$	$n + 1$
nido	B_nH_{n+4}	$n + 2$
arachno	B_nH_{n+6}	$n + 3$
hypho	B_nH_{n+8}	$n + 4$

Closo boranes lack the B-H-B 3c-2e bonds as there are equal amounts of boron and hydrogen atoms in the cluster making them thermally stable with moderate reactivity.[1] *Nido* boranes have less stability relative to *closo* with the one B-H unit less replaced by two hydrogen atoms shifting the electron density within the cluster.[15] A*rachno* boranes, with two B-H units less than *closo,* are highly reactive and unstable species at room temperature.[16]

Decaborane , $B_{10}H_{14}$ is a white crystalline powder, synthesized by the decomposition of diborane to produce a *nido* framework (n+2 skeletal electron pairs) with 10 terminal hydrogen atoms and four electron deficient B-H-B at the opened region of the molecule (Figure 1.1).[12] It slowly hydrolyzes in hot basic solutions and its aqueous solution is very acidic as a result of its B-H-B 3c-2e bonds.[1] The acidic bridged hydrogen atoms allow boron-6 (B6) and boron-9 (B9) to be more susceptible to nucleophilic attacks.[15] In contrast, the compound possesses considerable excess negative charge at B1, B2, B3, and B4 where these boron atoms can participate in electrophilic reactions.[15]

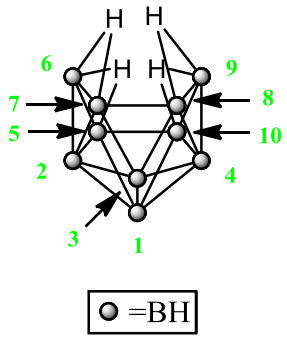

Figure 1.1- Decaborane numbering system of the boron atoms

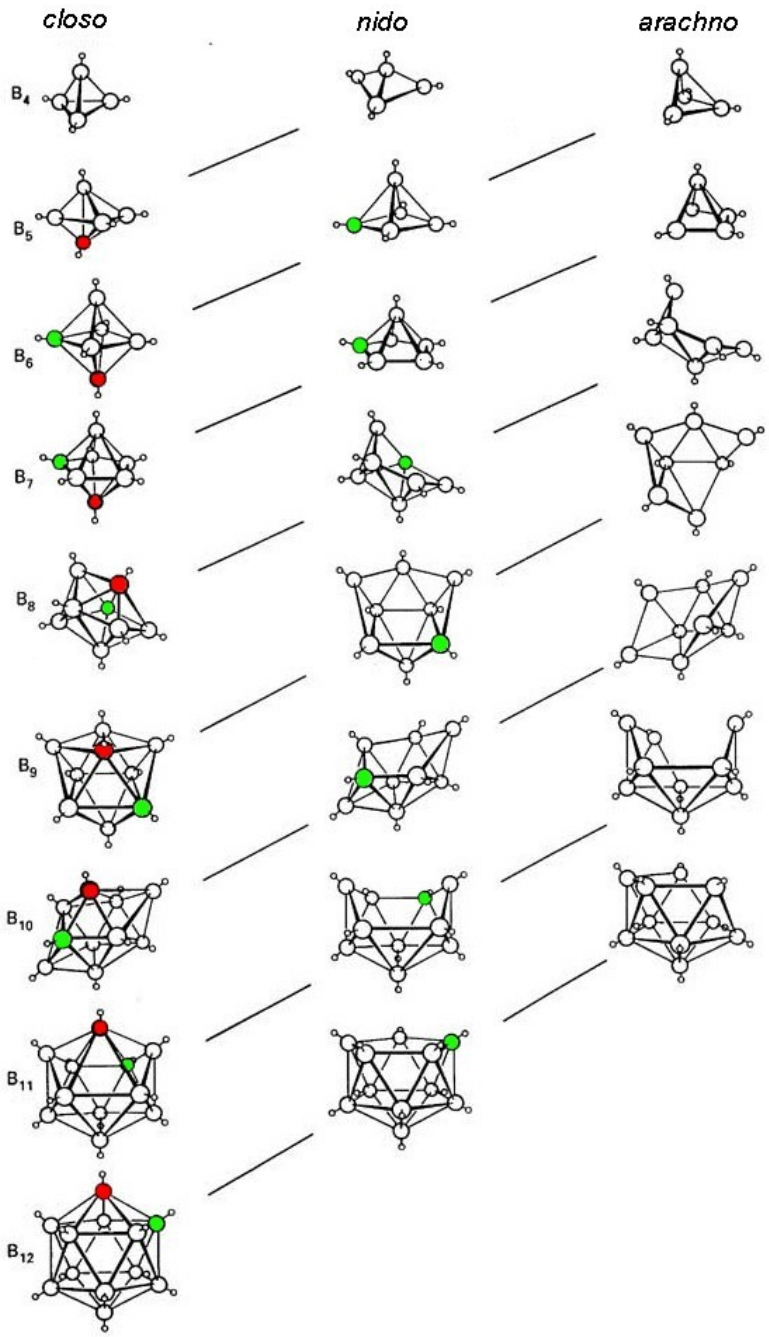

Figure 1.2[1] – Diagram of *closo, nido,* and *arachno* boranes (hydrogen atoms other than the BH framework are omitted). The red atom is omitted first followed by the green atom.

Many derivatives of boranes containing heteroatoms are known. These heteroboranes may be classified by exchanging a heteroatom for a BH_x group having the same number of valence electrons. Carboranes are species with a BH unit replaced by a CH (isoelectronic) unit have been the most popular polyhedral borane researched in the last 50 years.[13] It was originally researched to gain more control of the reactive boron hydrides such as B_2H_6 , B_5H_9 and $B_{10}H_{14}$ by incorporating carbons in the systems, converting them into organic derivatives.[17] Neutral CH groups are three-skeletal-electron donors when they replace BH groups in the cluster .[18] These systems have the ability to undergo substitution reactions at both the carbon and boron atoms without degradation of the carborane cage.[13] Investigations led to discovery that the most stable isomers contain the greatest separation between carbon atoms in the skeleton such as icosahedral carboranes.[17] An icosahedral neutral carboranes can be prepared with the formula $C_2B_{10}H_{12}$ -neutral *closo*. There are three possible isomer, 1,12-dicarbo-*closo*-dodecaborane (*para*-carborane), 1,7-dicarbo-*closo*-dodecaborane (*meta*-carborane), and 1,2-dicarbo-*closo*-dodecaborane (*ortho*-carborane). P*ara*-carborane is the most stable stability of all isomers; followed by *meta*-carborane and finally *ortho*-carborane (Figure 1.3).[17] Unlike many boron hydrides, icosahedral neutral carboranes are stable in the presence of oxidizing agents, alcohol, and strong acids and exhibit phenomenal thermal stability in temperatures up to 400^{o}C. [13] *Ortho*-carboranes can be synthesized by reacting acetylene with decaborane in the presence of a Lewis base such as acetonitrile, alkylamines and alkyl sulfide .[13] The other two stable isomers can be obtained by heating the *ortho*-carborane to 400-500^{o}C where it rearranges to the *meta*-carborane and at 600-700^{o}C it further isomerizes to para-carborane .[17]

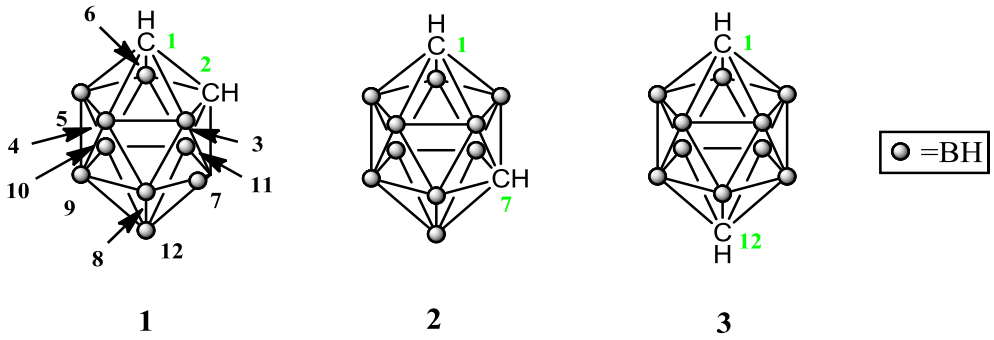

Figure 1.3 – Structures of the *ortho*-carborane (1), *meta*-carborane (2), and *para*-carborane (3). The numbers represents the position of each vertex of these icosahedral carboranes.

The electron density varies from one isomer to another with *para*-carborane bearing the highest electron density at the carbon vertices while the boron atoms all occupy the same level of density.[13] Due to the difference in symmetry of the other two isomers, the electron densities of meta-carborane and *ortho*-carborane, in decreasing order, are at positions 9 (10), 4 (6,8,11), 5 (12), 2(3), 1(7) and 9 (12), 8 (10), 4 (5,7,11), 3 (6), 1(2) respectively. [13] Hence, the CH groups in the carboranes are weakly acidic with pKAs of 22.0, 25.6 and 26.8 for *ortho*-, *meta*-, and *para*-carborane respectively.[19] They can readily be deprotonated to generate nucleophiles at the CH positions, whereas the boron vertices are susceptible to electrophilic substitution and direct electrophilic halogenation, alkylation, and sulfhydrylation.[13, 20]

Organic-inorganic block polymers

Organic-inorganic polymers are defined as hybrid polymers that are mainly composed of an organic component within a framework or network with inorganic groups tethered along the chain (Figure 1.4) .[21] These merged systems allow for the researchers to modify the properties of the polymer at the molecular scale by altering the inorganic and organic components.[2] There are two forms of organic/inorganic hybrid materials: (1) the inorganic and organic components are bonded covalently or ionically , or (2) the polymer form vesicles where the one component, depending on the solvent its dissolved in, is exposed to the exterior while the other is entrapped in the core of the structure.[2] The issues that arise with the latter include macrophase separation and leaching due to weaker bonds or lack thereof that are unable to hold the polymer(s) together.

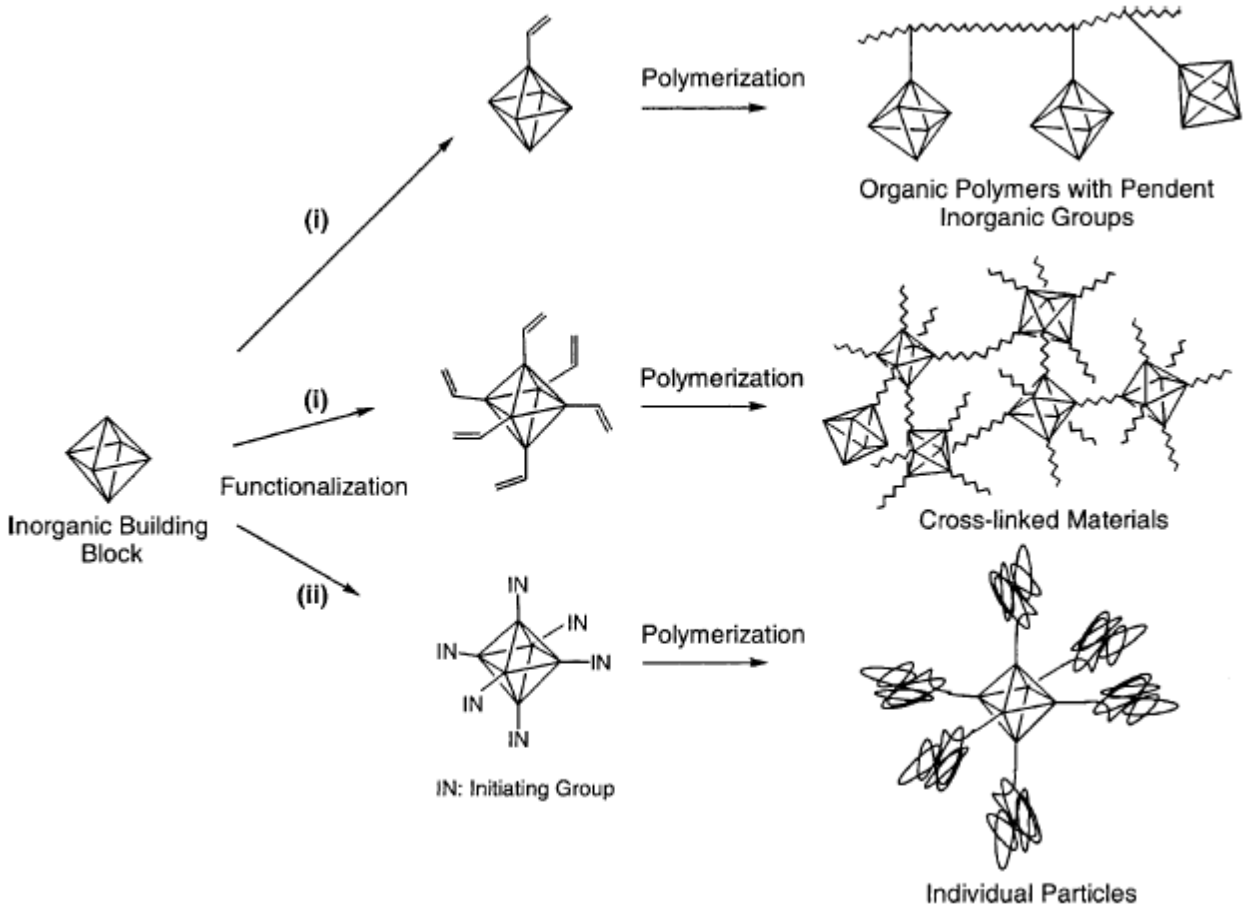

Figure 1.4 [2]- Schematic of various ways to functionalize an inorganic building block as a precursor from polymerization forming various forms of hybrid polymers.

Tethered silicon groups have captured the attention of material scientists due to their ability to synthesize hybrid organic-inorganic materials[22] ranging from a single silicon moiety to polyhedral silicon pendants. With a single silicon atom pendant covalently attached to the organic backbone, such as *tert*-butyldimethylsilyl groups (TBDMS), would increase phase separation of block copolymers causing specific morphology patterns in polar solvents.[23] Recently, polyhedral oligomeric silsesquioxane (POSS) molecules have been of interest for organic-inorganic hybrid block copolymers, possessing highly ordered morphologies at the nano-scale ranging from 10 to100 nanometers.[24] POSS molecules consist of a rigid cubic

structure composed of $R_8Si_8O_{12}$ where R represents the organic peripheries at each of the eight vertices. [25]

Self-assembly

Organic-inorganic polymers have the potential to form morphologies patterns ranging from small aggregates such as spherical to two-dimensional arrays such as lamellar. The simplest and most studied architecture of the linear AB block polymer models will be used to explain the formations of the patterns in microphase separation. These polymers have the capabilities to undertake formations in the melt or solvent evaporation that encompasses meso-, micro-, nano-phase separations depending on the length of the polymer.[3] Microphase separations are driven by chemical incompatibilities between the different A and B block of the copolymer.[3]

The size and the flexibility of the polymer influences the morphology patterns since it can slow down the diffusion, facilitate glassy dynamics and increase enthalpic barriers to allow copolymers to form shapes, while achieving phase equilibrium.[26] Flory and Huggins have developed an equation that represents the thermodynamics of polymer solutions entropy of mixing known as the Flory- Huggins interaction parameter (eq. 1).[3]

$$\chi_{AB} = (Z/k_BT)[\varepsilon_{AB} - (1/2)(\varepsilon_{AA} + \varepsilon_{BB})] \qquad (1)$$

Z represents the number of nearest neighbor monomers, k_BT represents thermal energy and ε_{AB} the interaction energy per monomer.[3] Positive χ_{AB} indicates that blocks in the polymer

experience more repulsion between both blocks. Conversely, negative χ_{AB} indicates a free-energy towards mixing as the blocks have similar properties.[3]

To characterize the block molecular structures, the degree of polymerization of the polymer represented by *N* accounts for the overall number of monomers units per polymer. Compositional fraction of a block $f_y = N_y/N$ where "*y*" corresponds to the block within the hybrid polymer reveals the amount of monomer unit of block "y" per polymer. A theoretical phase diagram for AB diblock copolymer compares the compositional fraction of block A (f_A) with respect to $\chi_{AB}N$ (*N* represents the degree of polymerization) of diblock copolymers as they self-assemble into different morphology patterns (Figure 1.5). [27] For symmetrical copolymers, both blocks occupy nearly equal volume fractions where $f_A = f_B = ½$ makes self-assembled alternating composition forming sheet-like domains known as lamellar (L). [28] As the ratio becomes more distorted with increasing f_A , the lesser B block aggregates into interior cylinders, leaving the longer A block on the exterior perimeter, forming hexagonally packed cylinder (C).[3] With further increase of the asymmetry, sphere domains are formed as smaller B interior blocks aggregate due to the smaller f_B . Gyroid phase (G) is a difficult phase to acquire as it is a small region that lies between lamellar and cylindrical regions.

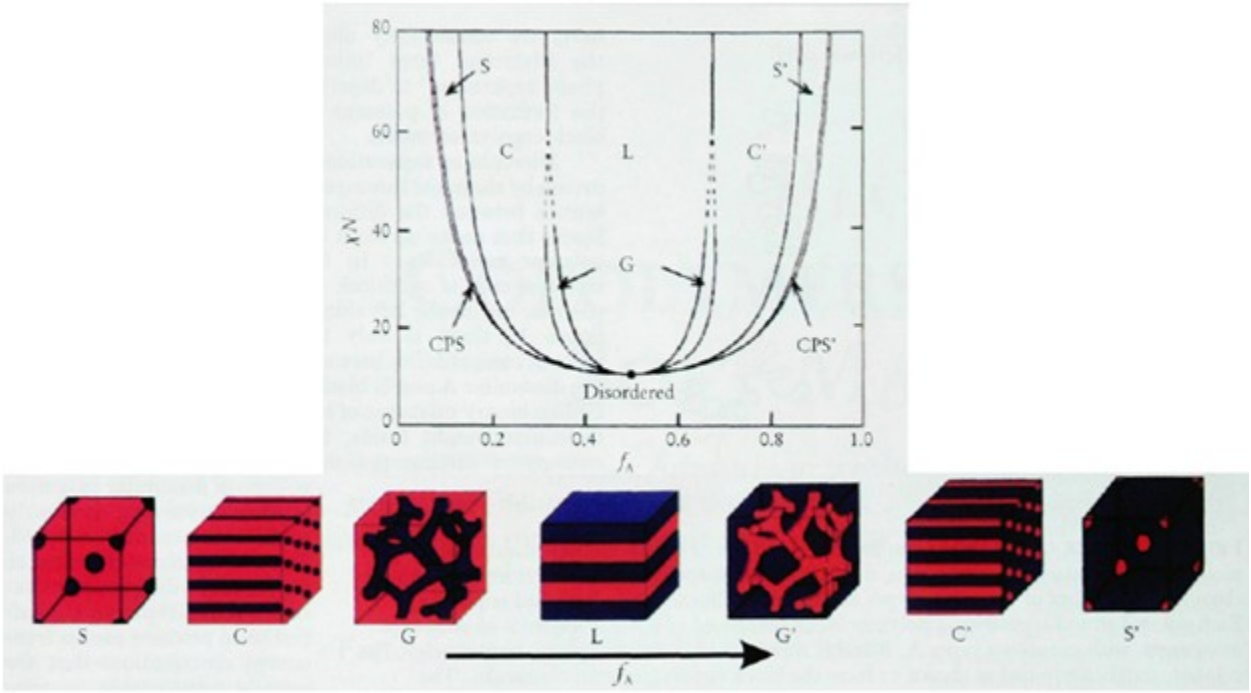

Figure 1.5 [3]- Theoretical phase diagram for linear AB diblock copolymers. (Upper) Four morphologies can be predicted: spherical (S), cylindrical (C), gyroid (G), and lamellar (L). (Lower) microdomain structures of f_A as it increases with fixed $\chi_{AB}N$ of a diblock copolymer.

Chapter 1.2: Material Characterization for Block Copolymers

The scanning electron microscope (SEM) is one of the most versatile instruments available for the examination and analysis of the microstructure morphology, chemical composition, crystalline structure and orientation of the sample.[29] A probe electron beam focuses and scans over the solid material surface.[30] Depending on the equipment, the electron beams range between 100 eV to 30 keV energy that has the power to focus as low as 10 Å.[30] The accelerated electrons from the beam carries significant amounts of kinetic energy that is dissipated as a variety of signals produced by the electron-sample interactions.[31] These interactions can be divided into two major categories: elastic interactions and inelastic interactions. Elastic interactions originate from the deflection of the incident electrons from the sample and by a wide-angle directional change of the scattered electrons.[29] Incident electrons that are elastically scattered through an angle of more than 90˚ are called backscattered electrons (BSE) and are responsible for illustrating contrasts in composition in multiphase samples.[29] Inelastic scattering interactions originate from the emission of low energy secondary electrons that escape from the sample.[30] Therefore, the amount of energy loss depends on the binding energy of the electron to the atom and whether the electrons from the sample are excited individually or collectively.[29] The secondary electrons contribute to the imaging of the sample by displaying its morphology and topography.[30] In addition to those signals, more information can be deduced for the x-rays, Auger electrons, and cathodoluminescence signals emitted from the sample.[29]

Differential scanning calorimetry (DSC) is a technique that monitors the heat flux between the sample and the reference pan, as the sample absorbs or releases heat as a function of temperature under specific atmosphere controlled by a program.[32] As it undergoes endothermic and exothermic phase transitions, peaks are displayed on the DSC. Thermal changes of a polymer, such as first order and second order transitions, can be identified from the plot include: glass transition (T_g), melting and boiling points, crystallization and temperature, percent crystallinity, fusion reactions, specific heat, oxidative/thermal stability, rate and degree of cure, reaction kinetics, and purity.[32]

The heat capacity of the sample can be determined from the DSC curve, as it displays a step-wise endothermic change indicative of a change in specific heat capacity of the polymer sample.[33] This signifies the glass transition temperature, where the amorphous phase of the polymer is transformed from a brittle, glassy material to a tough, rubber-like liquid.[32] As a result, with the temperatures above the glass transition temperature, the polymer experiences a higher heat capacity than below the glass transition.[32] As the temperature exceeds the T_g , a first order transition may occur, where heat is released and the exothermic transition phase occurs known as crystallization temperature (T_c).[32] As the sample is continuously heated, melting point (T_m) occurs as the crystals melt and enter an endothermic transition phase .[33]

Thermal gravimetric analysis (TGA) is a measurement used to determine weight change of a sample as a function of temperature in a controlled atmosphere.[32] The weight change can be quantified yet no information about the evolved gases can be determined unless it is couple

with mass spectrometer (MS) or Fourier transform infrared spectrometer (FTIR).[31] The decomposition of organic polymers under inert atmosphere produce smaller organic fragment that would display a degradation endothermic peak. However, under air or oxygen an exothermic peak would be displayed as a result of oxidation.[34] There are two kinds of thermal decomposition for polymers that may occur in separate occasions or combination called chain depolymerization and random decomposition.[35] With chain depolymerization, monomers and oligomers units are broken off the chain in a reverse process of polymerization that could be described as depropagation.[35] Conversely, random decomposition causes the chain to rupture and break at random points along the chain resulting in a various mixture of chain fragments.[35]

The derivative of the curve obtained by differential thermal analysis (DTA) can identify quantitatively at specific temperatures where the sample experiences weight loss or gain .[36] Polymers that experience weight loss at temperature prior to polymer degradation tend to include volatiles such as moisture, residual solvent, and oligomers.[34]

Gel permeation chromatography (GPC) is a technique used to determine the molecular weight distribution of polymers. This size exclusion chromatography separates analytes in the column based on its size of hydrodynamic volume.[37] The polymer is first dissolved into a HPLC grade solvent such as tetrahydrofuran (THF) or dichloromethane (DCM) and then injected in column packed with porous beads. As the column is washed with a solvent, the smaller polymer

analytes enters the pores and are retained longer than the medium and large size polymer analytes.[38] The larger polymer analytes are unable to fully settle inside the porous beads, therefore acquiring less retention volume and elute out of the column early .[38] Detectors are used to monitor the elution of the concentration of polymer analytes as they elute to collect their retention volume .[37] The information deduced includes the polymers purity, linearity, molecular weights and polydispersity index.[35, 37-38]

With linear homopolymers, polystyrene standards are used as the internal standard to calibrate and compare with the polymers studied.[35] Conventional single detector GPC instruments are inadequate for determining the molecular weights of block copolymer. Inadequate results would be obtained since the elution volume depends on not only the polymers molecular weights but the compositions of each block.[39] As a result, the polymers cannot accurately be measured since they are separated based on the size of the aggregated polymer in solution instead of their molecular weight .[40] The most common detectors sensitive to the concentration of the polymer are differential refractometry index (DRI), UV adsorption, and infrared absorption. With diblock copolymers, multiple detectors must be used simultaneously to establish the composition at each elution time and better estimate of the absolute molecular weight of the block polymer.[40] Combination systems such as DRI with low angle laser light scattering detectors (LALLS) or multi -angle laser light scattering (MALLS) are common since they both are molecular weight sensitive detectors.[41] A less expensive alternative is to collect information about the intrinsic viscosity (η) of the diblock polymer and calibration standards of both the polymers to construct a universal calibration curve tailored to

the block polymer sample.[39] Calibration using both the homopolymers of the diblock copolymer and create mathematical equations using the curves to estimate the molecular weights.[39]

Powder X-ray diffraction is a technique that uses Bragg's law to determine chemical composition and the crystal structure of crystalline and amorphous samples.[35] An x-ray beam with wavelength λ interacts with the electrons in the sample at angle θ where the beam is partially absorbed, transmitted, reflected and diffracted by the sample. [42] Diffraction and constructive interference occurs as the rays diffracted from the parallel planes with distances d, and the rays reflected from adjacent lines differ in path length by n, Bragg's law, $n\lambda=2d \sin\theta$ is satisfied (Figure 1.6).[43] The fine powder sample is scanned throughout a range of 2θ to detect all possible diffraction of the lattice that respects Bragg's law.[42] The rays are counted and peaks are plotted based on the d-spacings of the lattice planes.[35] The line width and shape of the peaks provide usable insight on properties of the sample such as particle size and identification of the elements in the sample.[43]

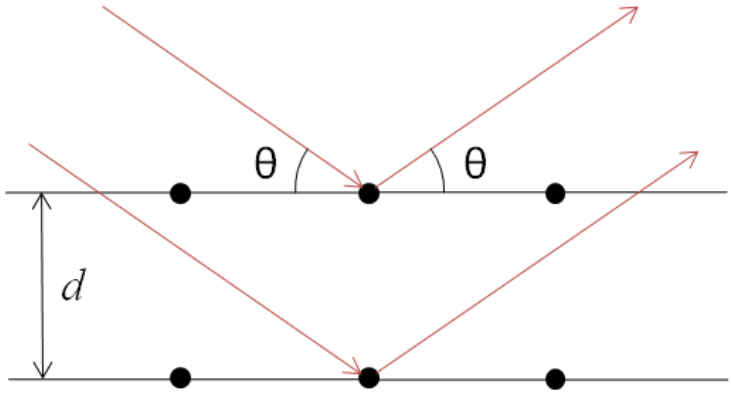

Figure 1.6[4]- Diffraction pattern from X-ray powdered diffraction (XRD) where θ represents the angle of incidence of the X-ray and d represents the spacing between the atom layers.

The degree of crystallinity of semi-crystalline /semi-amorphous polymers can be explored using XRD.[35] The crystalline portions of the polymer sample would give sharp narrow diffraction peaks as opposed to the broad halo peaks caused by the amorphous portion.[35] To identify the percentage of crystallinity within a prepared sample, the ratio of the intensity of sharp versus broad peaks can be calculated.

Chapter 2: Carborane Raman Reporters

Introduction

The development of powerful cellular imaging systems has allowed for quantitative analysis of cellular events and visualizations of relevant cellular interactions. Among these imaging systems, Surface-enhanced Raman scattering (SERS) microscopy allows for biological imaging in drug discovery and treatment.[44] SERS utilizes molecules suitable for detection by Raman spectroscopy which absorbs on metal surfaces promoting strong vibrational signals.[45] Raman scattering or Raman spectroscopy relies on inelastic scattering of monochromatic light typically from a laser source revealing information about the vibrational, rotational, and other low-frequency modes in a system.[46] Photons of the laser are absorbed by the sample and polarizes the electrons in the nuclei to an unstable excited state known as *virtual state,* and quickly re-irradiated returning to ground state.[44] Frequency of reemitted photons are shifted up or down in comparison to the original path of monochromatic light producing a Raman effect (Figure2.1).[44]

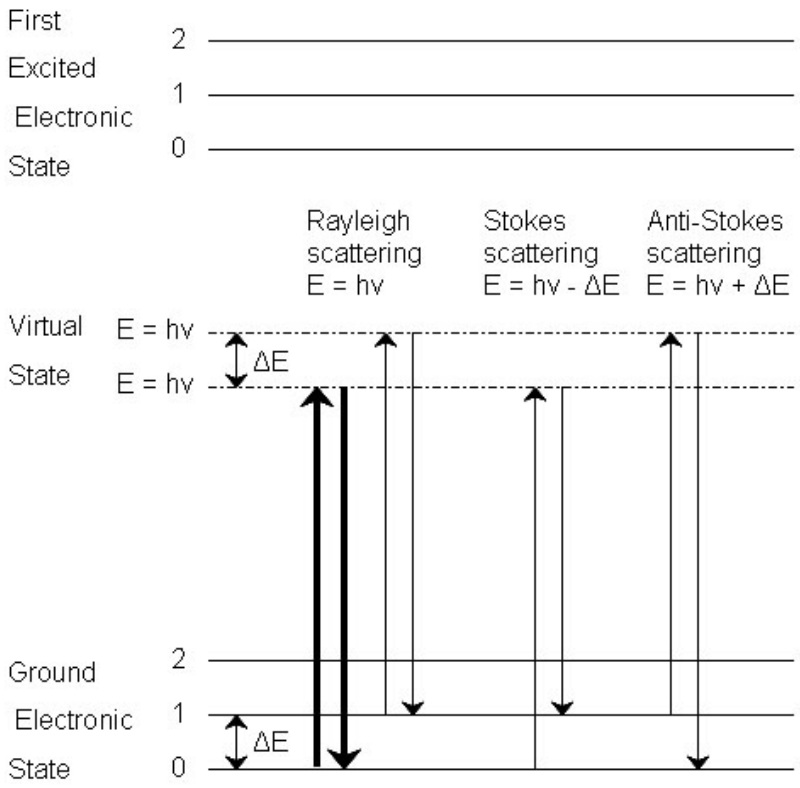

Figure 2.1[5]- The three types of scattering by a molecule excited by a incident light beam. Rayleigh scattering the molecules excited returns back to its original state. Stokes and Anti-stokes scattering differ in energy by ΔE.

Raman reporter research developments have been recently emerging as an alternative to fluorescence-based spectroscopy in bioimaging and therapeutic studies.[47] SERS probes can improve bioanalysis as it can minimize photobleaching, peak-overlapping, and low signal-to-noise ratio associated with complex biological systems. [48] The challenge of synthesizing these probes are hindered by the availability, sensitivity, and reproducibility of Raman-active compounds especially in the near-infrared region.[49] Crystal violet, malachite green isothiocyanate and Nile blue are common Raman-active molecules used to detect signals within the visible and ultraviolet region. [50] Raman-active molecules producing signals in the UV/Vis

range risk of blending with signals generated by cellular compounds less effective for *in vivo* imaging.[46]

The energy changes detected in vibrational spectroscopy are required to cause nuclear motion or displacement, meaning the monochromatic laser light with frequency v_o excites the molecules and transforms them into oscillating dipoles that emit light at three different frequencies.[47] The dominant process occurs when only the electron cloud distortion is involved in scattering and the photons merely experiences minimal frequency change as the electrons are comparatively light.[47] This scattering is known as the elastic Rayleigh scattering process where a molecule with no Raman-active modes absorbs a photon with the same frequency v_o.[44] The more subdued inelastic scattering occurs when nuclear motion is induced during the scattering where the energy of the scattered photon differs from the original incident photon, the frequency is said to be Stokes or Anti-Stokes.[49] The Stokes Raman frequency scattering signifies a reduced scattered light as the photons' energy is transferred to the Raman-active mode with the frequency v_m.[47] Conversely, Anti-Stokes frequency corresponds to a photon when the frequency v_o is absorbed by a Raman-active molecule already in the excited vibrational states where excess energy is released from the Raman-active modes returning to the basic vibrational state. The inelastic scattering is a weak process where only 0.001% of Raman signals are produced opposed to Rayleigh scattering attains 99.999% of

incident photons.[44] Due to the Raman scattering weak signals, special measures must be taken to decipher the inelastic frequencies from the dominant Rayleigh scattering frequencies.[44]

To obtain high quality Raman signals, SERS technique can be applied to increase the Raman signals to approximately 6 orders of magnitude stronger.[44] A Raman-active molecule binds to an etched metal surface, generally silver or gold substrates, and enhances the Raman signal by chemical and/or electromagnetic enhancement.[51] These two metal surfaces are best since their plasmon resonance frequencies fall within the visible and near-infrared light matching the radiation used to excite Raman modes.[51]

The intensity of Raman signals proportional to the square of the electric dipole moment $P= \alpha E$ yet, the exact mechanism of this enhancement is controversial. The enhancement of both the polarizability α and the electrical field E are plausible theories to SERS.[52] The chemical enhancement is speculated to be the cause of a bond between the molecule and the metal surface that produces surface metal ions.[47] This facilitates the charge transfer from the metal surface to the molecule.[44] As a consequence, the surface species will increase the molecular polarizability of the molecule and enhance it to new electronic states where it is believed to resonant intermediates in the Raman scattering.[47] However, the effect of chemical enhancement is limited to monolayer coverage of the directly bonded molecules.[44]

Electromagnetic enhancement is the other possible theory to the Raman signal enhancement that accounts for the interaction between the laser beams with irregularities on the roughened

metal surface.[51] In the case of silver surfaces, they are covered with electrons held in the lattice by the presence of positive charge from the silver metal centers.[53] As a result, the electron density extends allowing considerable movement along the surface.[51] As the electrons interact with the laser beam, surface plasmon occurs as the clusters of electrons begin to oscillate across the surface.[51] The Raman-active molecule is surrounded by freely moving electron cloud that intensifies the polarizability of the surface electrons causing greater polarization around the molecule.[44] Strong field enhancement occurs when the plasmon frequency is perpendicular to the surface as oppose to parallel.[52] With the appropriate laser frequency, part of the surface between particles become extremely active to the point at which two particles touch, as known as "hot spots", an enormous electric field is generated and will give effective SERS.[52] Therefore, the frequency chosen for the particle size and shape and the way the particles organize in clusters will contribute to the SERS enhancement.[52] In contrast to the chemical enhancement theory, by definition, electromagnetic enhancement can occur from the first or subsequent layer of molecules attached to the metal surface.[44]

Kennedy *et al.* reported the discovery of water-soluble silver nanoparticles (NPs) co-functionalized with carborane and tumour cell targeting antibodies. This discovery serves two functions where the multiplex provides SERS detection *in vivo* combined with drug delivery.[46] They demonstrated the unique ability to functionalize silver NPs with a derivatized *ortho*-carborane as the Raman reporter and conjugated antibodies specific to epidermal growth factor receptor (EGFR) overexpressed on cancer cells.[6] Apart from the SERS detection, these

functionalized NPs have the potential to be considered for boron delivery in the search for Boron Neutron Capture Therapy (BNCT) that will be discussed in further detail later in this chapter. The NPs were designed to incorporate three requirements: (1) conjugate suitable Raman-active molecules, (2) bond molecules specific for EGFR interaction in cancer cells, and (3) obtain solubility properties appropriate for cellular environments(Figure 2.2).[6]

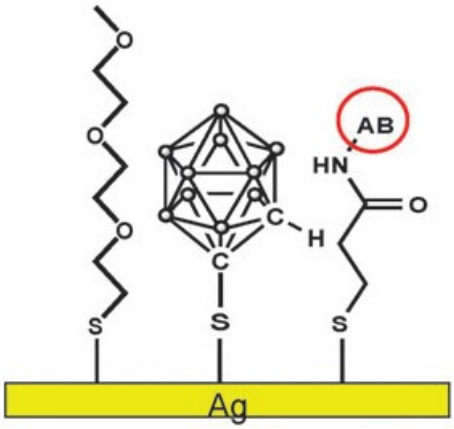

Figure 2.2[6]- Diagram of the silver NP with *ortho*-carborane thiol, thiolated secondary antibody, and thiolated polyethylene glycol (PEG) chains.

The ideal Raman-active molecules for bioimaging are molecules that detect signals in regions that are not common for molecules in the intracellular or extracellular environments.[53] The polyhedral heteroborane clusters, such as carboranes, contain a B-H Raman stretch signals positioned in the mid-infrared range where they can serve as unambiguous Raman/SERS reporters.[54] A monosubstitued thiol-*ortho*-carborane (*o*-carborane) was synthesized and bound to 25 nm silver NPs.[6] The SERS spectra obtained demonstrated a high intensity B-H stretch between 2550-2650 cm^{-1}.[55] Thiolated polyethylene glycol (PEG) chains were bound to

the NPs making the complex water-soluble, thus allowing it to be sustainable in cellular environments.[6, 56] These relatively inert thiolated chains acts as fillers between the carboranes hindering reactions with one another.[6] Lastly, thiolated secondary antibody directed towards detecting anti-EGFR antibodies on the cell surface of cancer cells were functionalized onto the NPs.[6] Thiosuccinimidyl proprionate are ligands bound to the NPs with an activated ester group at the extremity of the ligand used to bind EGFR antibodies.[6]

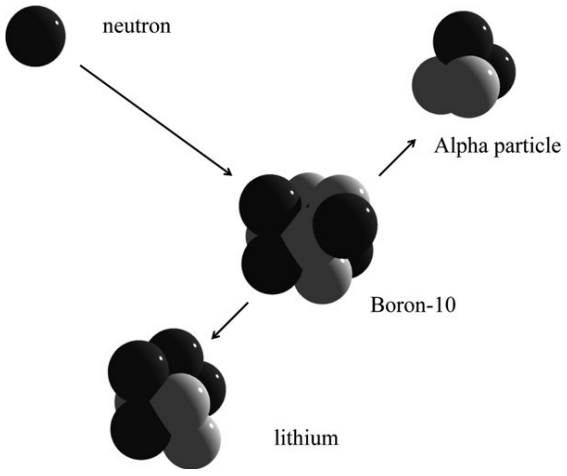

Figure 2.3[7]-Boron neutron capture nuclear reaction between ^{10}B and thermal neutrons with the release or $^{7}Lithium$ and alpha particles.

The therapeutic contributions of these NPs multiplex were tested to discover whether or not it could be used simultaneously for drug delivery for BNCT. BNCT is a binary method for cancer treatment , which is based on the nuclear reaction of two essential nontoxic species: nonradioactive ^{10}B isotope and low-energy thermal neutrons.[57] It irradiates tumour cells at precise locations that may not be fully known such that residual cancer cells do not become the foci for tumour reoccurrences.[58] The nuclei of ^{10}B possess an unusual capacity for absorbing thermal neutrons.[59] These neutrons are irradiated by a neutron source at 0.025 eV where the absorption by the atom's nucleus produces an activated nucleus that undergoes prompt fission generating lethal energetic particles causing cell death (Figure 2.3).[57] This cancer therapy focuses on tumours that are resistant to all current forms of therapy including surgery, chemotherapy, radiotherapy, immunotherapy and gene therapy.[60] To date, there are two leading low-molecular BNCT agents used in clinical trials for brain tumour: sulfhydryl borane (BSH) and p-dihydroxyboryl-phenylalanine (BPA) (Figure 2.4).[61]

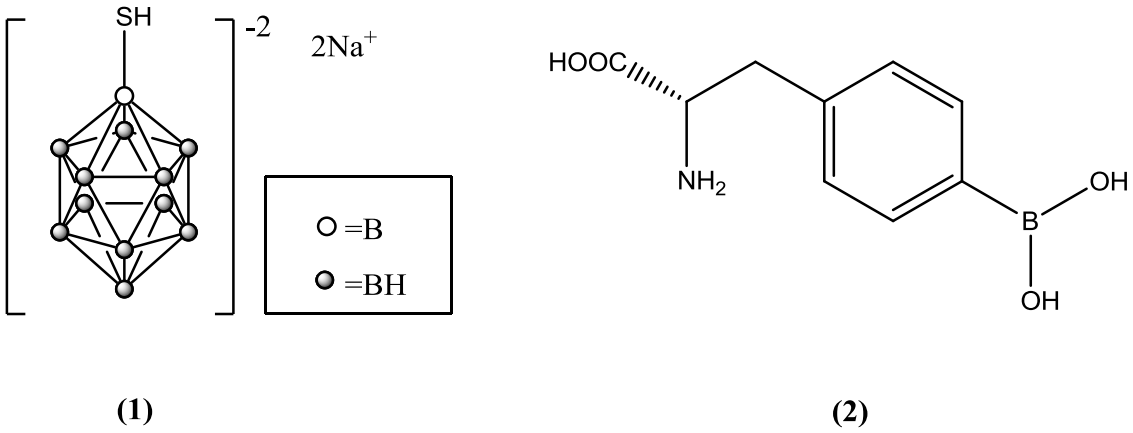

Figure 2.4- Current leading BNCT agents (1) sulfhydryl borane Na2B12H11SH (BSH) and (2) p-dihydroxyborylphenylalanine (BPA).

Despite the results of these compounds, ongoing research is currently being conducted for more efficient compounds. Several criterions must be incorporated in the molecules to surpass the results of BSH and BPA. A major criterion is to achieving tumour concentrations in the range of 20-30µg of ^{10}B/g or 10^9 of ^{10}B atoms/cell.[60] At these concentrations, the neutron beam energy used in the capture reaction may be reduced to values below the threshold of developing neutron capture by ^{1}H and ^{14}N atom in the body.[62] Secondly, these boronated compounds must concentrate and persist in the tumour cells while blood values fall to low levels, otherwise BNCT will cause non-selective damage to both the tumour and its surrounding healthy blood vessels.[63] Sufficiently low toxicity is required to ensure the dose administered would be tolerated, first in animal models in the early stages of the clinical trials procedure and subsequently in patients.[64] As for tumours in the central nervous system, some level of hydrophobicity must be incorporated in the BNCT agents to cross the blood brain barrier.[65]

With these parameters in mind, the 25 nm silver NPs were loaded with 45% of *o*-carborane thiol, 10% of the thiosuccinimidyl propionate tethered to secondary antibodies and remaining available surface with the thiolated polyethylene glycol chains.[6] The co-functionalized carboranes were estimated to deliver 5000-10 000 carborane molecules to the antigenic sites in hopes of achieving the 10^9 boron atoms per cell to satisfy the total load demand of 1000 boron atoms of 100 carborane molecules per site where each cell average 10^6 antigenic sites.[6] Although 45% of carborane per nanoparticle carrying well over the 100 carboranes requirement by 90 times, considerably low amounts of NPs were detected on the 10^6 target sites.[6] High loading of boron was achieved but its inability to bind to all the receptors is suspected to due to the formation of homo-dimer and oligomers EGFR receptors that are in very close proximities.[55] EGFR receptors that are within the proximities of 8 nm or less caused an issue since the 25 nm NPs were unable to bind to more than one receptor per EGFR receptor cluster.[66]

The silver NPs also have the potential to be used for photothermal therapy and undergo two-photon luminescence with the laser power increased the intensity of the incident laser from 10mW to 50mW.[67] The increased intensity allow the particles to absorb more energy creating heat sources where thermal ablation therapy can occur as reported using gold-nanoparticle with anti-EGFR conjugated on the surfaces.[67]

This portion of the thesis research project began with attempts to synthesize new and improved carborane derivatives with a tethered nitrile group as second Raman-active

functional group on the NP. The motivation stemmed from the previous success of by the Pezacki group incorporating a nitrile group for SERS bio-imaging.[24]

Results and Discussion

1,12- bis(mercapto) -*p*-carborane and 1,7- bis(mercapto) *m*-carborane were synthesized using similar procedures. Both *p*-carborane and *m*-carborane were purchased from Katchem and were not purified before use. The CH bonds were deprotonated using 2.2 equivalent of cold 1.6 M butyllithium under inert atmosphere and stirred for 1 hour to produce the carboranyl carbanion. Elemental sulfur was added in increments over a period of 10 minutes and the reaction was stirred overnight at RT. The colour changed from yellow to white indicating an S_N2 reaction occurred with the carboranyl carbanion attacks the sulfur creating dithiolate carborane. The solvent was removed via rotovap and re-dissolved in water. The mixture was acidified with 4.0M HCl to pH 1.00 to hydrolyze the dilithio salt resulting in the bis(mercapto) species producing a white precipitate. The precipitate was extracted with hexanes and then dried over magnesium sulfate. The hexanes were removed via rotovap producing a white powder with 71% yield. The ^{1}H NMR spectra displayed broad multiplet peaks between 4.00-0.50 ppm to account for the 10 carboranyl BH hydrogens and a singlet at 3.05 and 3.41 ppm for SH of the bis(mercapto) -*p*-carborane and bis(mercapto) *m*-carborane respectively (Appendix Figure A1). The broad multiplet peaks of the BH are the result of boron-11 and boron-10 having a 3/2 and 3 spin respectively. The BH would experience splitting patterns of a quartet from boron-11 and a septet for the boron-10 with 4:1 intensity peaks respectively. Thiol-carboranes will provide a strong silver-sulfur bond to the silver NPs to ensure the carborane remains attached.

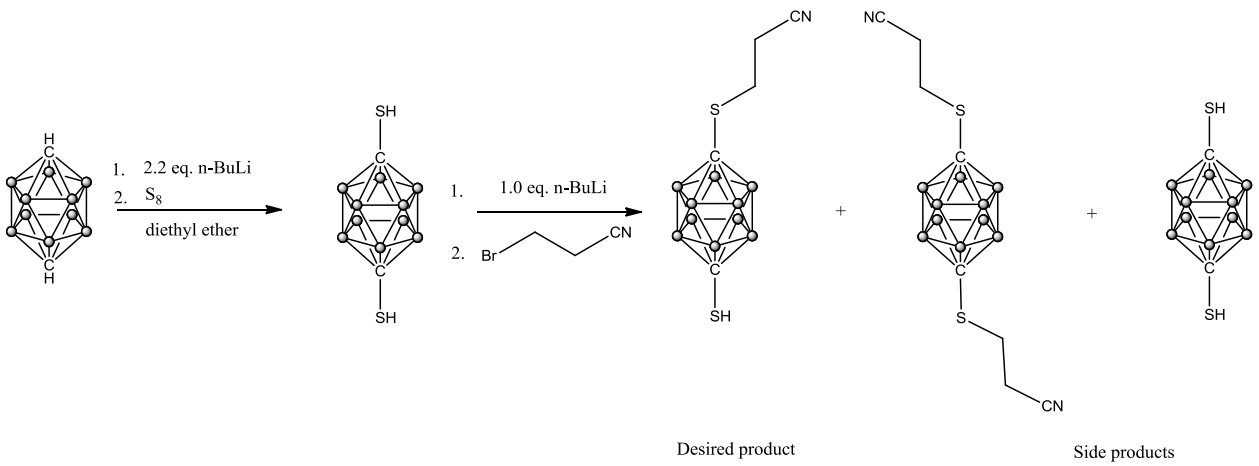

Scheme 2.1- Reaction scheme of the synthesis of 1,12- bis(mercapto) -*p*-carborane follow by the synthesis with 3-bromopropionitrile to produce 1-(1-thiopropionitrile)-12-mercapto-*p*-carborane

Attempts to establish a mono-S-substituted-propionitrile using bis(mercapto) -*p*-carborane and bis(mercapto) *m*-carborane were explored (Scheme 2.1). Limiting the reaction to mono-substituted thiol-carboranes is essential to allow the thiol to bond to the silver NPs. The procedure first involved 1,12- bis(mercapto) -*p*-carborane (or 1,7- bis(mercapto) *m*-carborane) dissolved in dry diethyl ether under inert atmosphere and allowed to react with 1 equivalent cold 1.6M butyllithium. The reaction mixtures were stirred for 1 hour to ensure deprotonation of one thiol group. Subsquential addition of 3-bromopropionitrile was added to the mixtures and stirred for 4 hours at RT. The solvent was removed via rotovap and product was re-dissolved in water. The product was acidified with 4.0M HCl to pH 1.00 to protonate the RS^-

anions. The aqueous solution was extracted with hexanes (3 X 20 mL) and dried over magnesium sulfate. The final product was a light yellow oil with a crude yield of 40% for the *p*-carborane derivative (and 64% *m*-carborane derivative). The ^{1}H NMR spectra of the mixture displayed broad multiplet from the BH bonds between 3.50-0.50 ppm (Appendix Figure A2). The CH_2 methylene peaks were at 2.77 and 2.51 ppm for the *p*-carborane derivatives (2.96 and 2.60 ppm for the *m*-carborane derivatives). Unfortunately, the mono-thiol peaks could not be distinguished in the spectrum. GC-MS conducted with these oils showed that side-products were present in the crude. Attempts to isolate the desired compound via column chromatography were unsuccessful as the products reacted and decomposed with the silica gel. Other isolation techniques such as recrytallization and extraction were also not successful.

Experimental

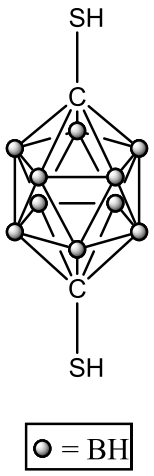

1,12- bis(mercapto) -*p*-carborane

Para-carborane (0.086g, 0.596 mmol) was dissolved in 8 mL of dry diethyl ether under inert atmosphere. 2.2 equivalent of cold 1.6 M n-butyllithium (0.820mL, 8.71mmol) was added dropwise and stirred for 1 hour. Sulfur (0.039g, 1.22 mmol) was added and stirred overnight where the solution changed from yellow to white. The solvent was removed *in vacuo* and re-dissolved in 5 mL of distilled water. The reaction mixture was acidified to pH 1.00 with 4M HCl to afford a white precipitate. The reaction mixture was washed with hexanes (3 X 20 mL). The organic layers were combined and dried with Mg_2SO_4. The hexanes were removed *in vacuo* to afford a white powder with 71% crude yield.

^{1}H NMR, (400 MHz, $CDCl_3$) δ 3.17-0.80 (br m, 10H, BH), 3.05 (s, 2H, SH)

Mass spec m/z : 208.35 found : 208.1

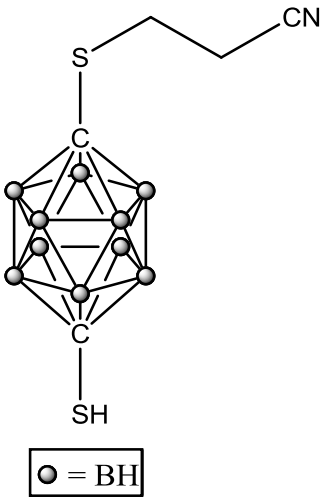

1-(1-thiopropionitrile)-12-mercapto-*p*-carborane

1,12-Dimercapto-*p*-carborane (0.035g, 0.168mmol) was dissolved in 8 mL of dry diethyl ether under inert atmosphere. 1 equivalent of 1.6M of cold n-butyllithium (0.11mL, 0.168mmol) was added and stirred for 1 hour. 3-bromopropionitrile (0.010mL, 0.168mmol) was added to the solution mixture and stirred for 4 hours. The solvent was removed via rotovap and re-dissolved in 5mL of distilled water. The reaction mixture was acidified to pH 1.00 with 4M HCl to afford a white precipitate. The reaction mixture was washed with hexanes (3 X 20 mL). The organic layers were combined and dried with Mg_2SO4. The hexanes were removed via rotovap to afford a crude light yellow oil with a 40% yield.

^{1}H NMR, (400MHz, $CDCl_3$)δ 3.50-0.50 (br m, 10H), δ 2.77(td, 2H, J= 7.2 Hz, 1.76Hz), δ 2.51 (td, 2H, J= 7.2 Hz, 1.76Hz)

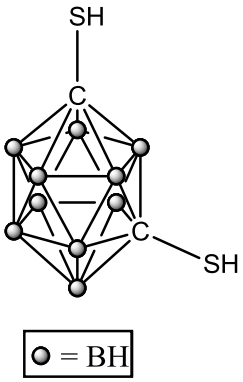

1,7-bis(mercapto)-*m*-carborane

Meta-carborane (0.095g, 0.659 mmol) was dissolved in 8 mL of dry diethyl ether under inert atmosphere. 2.2 equivalent of 1.6 M of cold n-butyllithium (0.91mL, 1.46 mmol) was added dropwise and stirred for 1 hour. Sulfur (0.046 g, 1.44 mmol) was added and stirred overnight where the solution changed from yellow to white. The solvent was removed *in vacuo* and re-dissolved in 5 mL of distilled water. The reaction mixture was acidified to pH 1.00 with 4M HCl to afford a white precipitate. The reaction mixture was washed with hexanes (3 X 20 mL). The

organic layers were combined and dried with Mg_2SO_4. The hexanes were removed *in vacuo* to afford a white powder with 60% yield.

^{1}H NMR, (400MHz, $CDCl_3$) δ 4.01-0.72 (bra m, 10H), δ 3.41 (s, 2H)

Mass spec m/z : 208.35 found :207.4

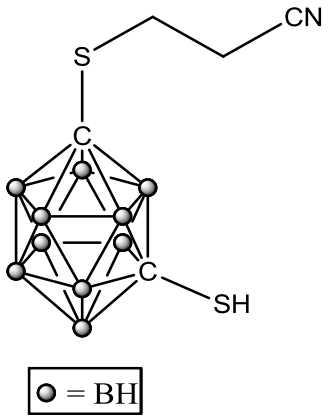

1-(1-thio-propionitrile)-7-mercapto-*m*-carborane

1,7-Dimercapto-*m*-carborane (0.131g, 0.628 mmol) was dissolved in 8 mL of dry diethyl ether under inert atmosphere. 1 equivalent of 1.6M of cold n-butyllithium (0.39mL, 0.630mmol) was added and stirred for 1 hour. 3-bromopropionitrile (0.06mL, 0.65 mmol) was added to the solution mixture and stirred for 4 hours. The solvent was removed via rotovap and re-dissolved

in 5mL of distilled water. The reaction mixture was acidified to pH 1.00 with 4M HCl to afford a white precipitate. The reaction mixture was washed with hexanes (3 X 20 mL). The organic layers were combined and dried with Mg_2SO_4. The hexanes were removed via rotovap to afford a crude light yellow oil with a 64% yield.

^{1}H NMR, (400MHz, $CDCl_3$) δ 4.00-0.60 (br m, 10H), 2.96 (t, 2H, J=7.6 Hz), δ 2.60 (t, 2H, J=6.8Hz)

Chapter 3: Organic- Organodecaborane block copolymers

Introduction

Organic-inorganic block copolymers possess the ability to phase segregate to tunable materials that are affected by the nature of the monomers, the relative chain lengths, the degree of polymerization, and the solvent employed for slow solvent evaporation. Living polymerization is a technique used to synthesize these block copolymer using atom-transfer, radical polymerization, reversible addition-fragmentation chain- transfer polymerization, and of course ring opening metathesis polymerization (ROMP)[68]. This chain growth polymerization requires the activation of a catalyst that further activates monomer species until the monomer supply is exhausted. The addition of the monomers starts a cascade or propagation reaction reestablishing a monomeric active species at the terminus of the chains. With living polymerization, catalytic conversion does not undergo termination without the addition of a chain-terminal agent which leads to the irreversible disappearance of the active centers.

ROMP catalysts in the recent years have evolved to allow well-defined block copolymer with controlled molecular weights and stereostructures to be synthesized.[69] Although olefin-metathesis catalysts such as [(*t*BuO)$_2$(ArN)Mo=Ch(*t*Bu)] and Grubbs 1 (**1**) are capable of achieving controlled living polymerization making ROMP, this novel technique to synthesize polymers has been limited by the functional groups on the monomer as they get moderate PDIs of around 1.2 (Figure 3.1).[70] Grubbs 1 can also be deactivated by strong coordinating solvents such as acetonitrile, DMF and DMSO producing mixtures of ruthenium complexes.[71] In the presence of carbon monoxide, functional groups of the monomers such as alcohols and primary

amines have shown to destabilize the ruthenium complex resulting in decompositions of the catalyst.[72]

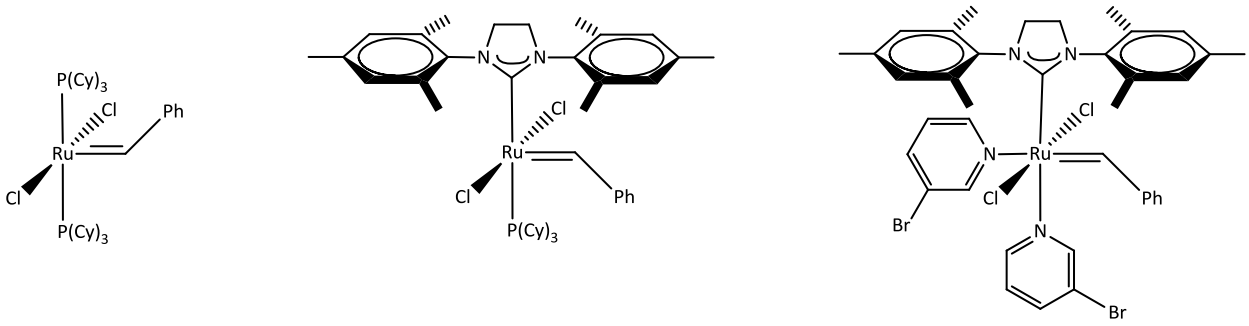

1 2 3

Figure 3.1- Three different generations of Grubbs catalysts. First generation of Grubbs (1), Second generation of Grubbs (2), and Third generation of Grubbs (3).

So called "Grubbs 2" is the second generation of these ruthenium catalyst where PCy_3 ligand is substituted by a significantly larger and more electron donating N-heterocyclic carbene (NHC) ligand **(2)** (Figure 3.1)).[73] The latter exhibits significant increase in reactivity with olefin monomers relative to Grubbs 1. [74] This ligand upgrade provides an increase the labilization of the phosphine ligand due to the large trans-effect but the rate of initiation was unfortunately slower than (1).[75]

Mechanistic studies of both Grubbs 1 and Grubbs 2 showed the lack of control of molecular weight distribution using ROMP with highly strained monomers .[76] The rather large discrepancy between a slow rate of initiation (k_i) and a much faster rate of propagation (k_p) of polymerization results in back-biting and chain-transfer reactions diminishing the uniformly of the polymer chains.[74]

Block copolymers are easily synthesized by ROMP utilizing the third generation Grubbs catalyst .[77] The Grubbs 3 (**3**) catalyst bears an N-heterocyclic carbene and two 3-bromopyridine ligands have shown to significantly increase the catalysts' reactivity and controlled living polymerization for a wide range of functional groups on a norbornenyl backbone (Figure 3.1).[70] The 3-bromopyridine ligands as opposed to PCy_3 originally in Grubbs 1 and 2 , enables the dissociation from the ruthenium core at rapid speeds as well as slow rebinding increasing the catalytic turnovers. [78] The combination of the electron–deficient ligand accompanied with its dissociation and rebinding abilities increases the turnover rates making this catalyst highly reactive.[78]

The rate of initiation of Grubbs 3 surpasses that of Grubbs 2 by at least six order of magnitude making it the fastest initiation rate in a ruthenium-based system.[79] A linear relationship exists between the monomer/catalyst and the number average molecular weight which demonstrates the control of molecular weight where Grubbs 3 rate of initiation/rate of propagation (k_i/k_p) ratio is high enough that all the chains initiate and grow at similar rates.[70] The extremely high rate of initiation and high rate of propagation surpasses those of Grubbs 1 resulting in a narrow PDI (<1.1) and good molecular-weight control.[78]

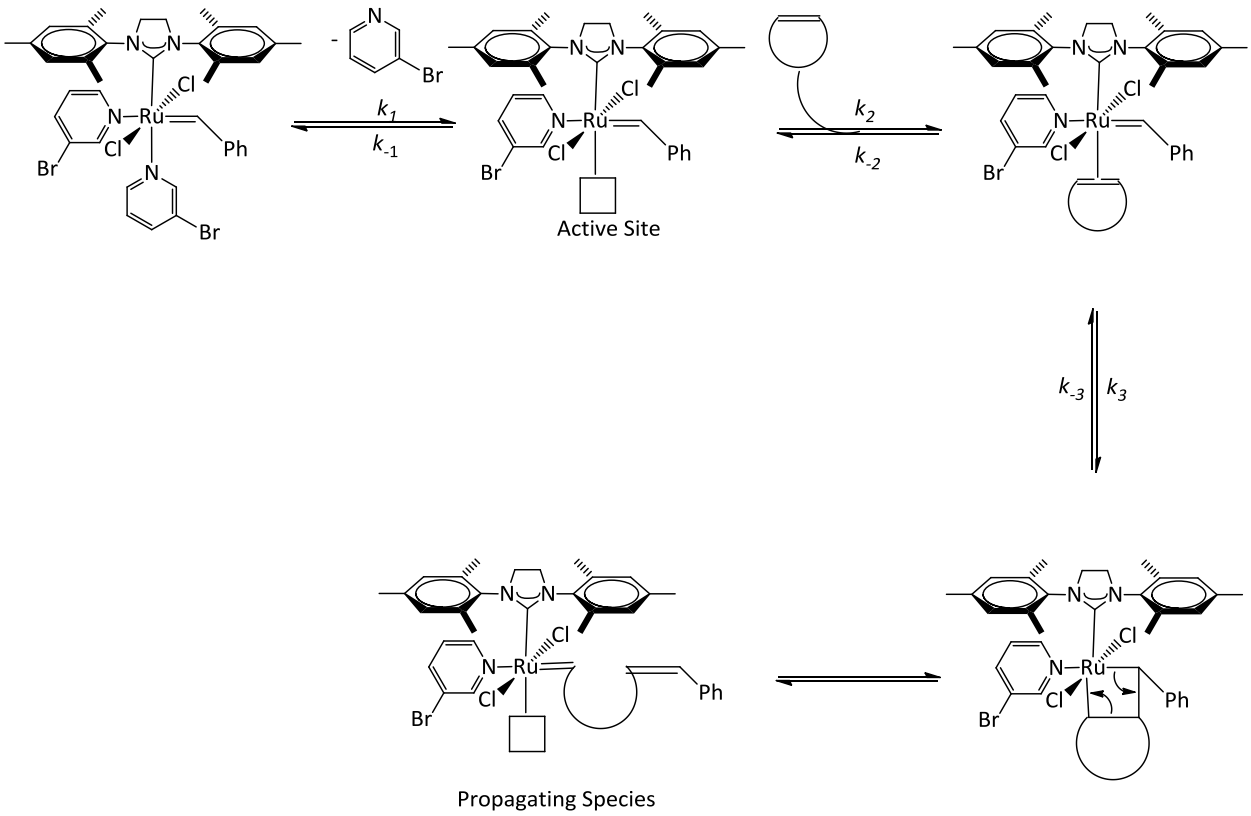

Scheme 3.1- Catalytic process of the activation of Grubbs 3 and its intermediate species.

In addition, this catalyst has demonstrated high efficiency in molar conversions closely matching the theoretical molar feed of the monomers. It has been demonstrated that initiation rate constant increases linearly with Grubbs 3 with molar concentration reaching as high at 3750 equivalents of olefins attesting that the kinetics of these reaction conditions remains nonsaturated.[78]

The monomers of choice for ROMP have traditionally been norbornene derivatives due its high strain energy, availability, and simple synthetic path. Polymerization of the parent bicyclic ring norbornene requires cryogenic conditions to slow the reaction rate in order to acquire low PDI.[70] Various derivatives of norbornene containing a combination of heteroatoms, bulky

moieties, cyclic groups have been successfully synthesized into homopolymers, block copolymers, and block tripolymers with PDI reaching well below 1.2 .[74] These substituted norbornenes , depending on presences of heteroatoms and/or bulky groups allow the polymerization reaction to be conducted in conditions from ambient temperatures to 50^{o}C.[80]

Hybrid organic—inorganic block copolymers behave in a similar fashion as surfactants when dissolved in various solvents. Fewer reports on norbornene derivatives with inorganic pendant have been published compared its organic counterparts. Inorganic norbornenyl derived monomers containing tethered main group elements as well as transition metal moieties have been synthesized in the past.[81] [81a] Sneddon et *al.* have reported the synthesis of 6-(5-norbornenyl-decaborane (NDB) via hydroboration resulting in two isomeric exo and *endo* forms (Scheme 3.2). *[82]* These decaborane derivatized monomers can be prepared using the titanium–catalyzed hydroboration reaction based on Hartwig's catalytic cycle as summarized by Scheme 3.3.[83]

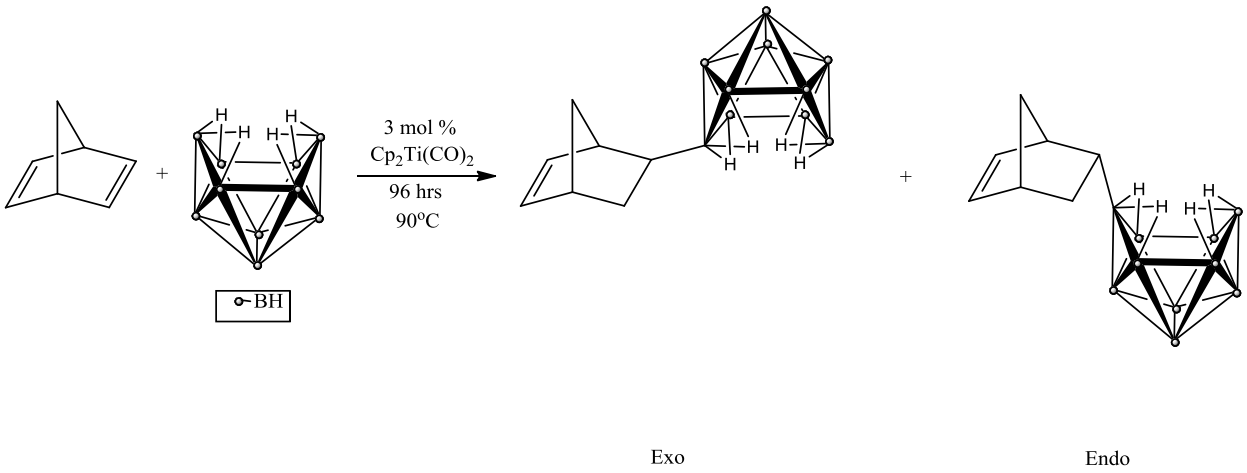

Scheme 3.2- Reaction Scheme of hydroboration of decaborane and norbornadiene catalyzed by 3% mol of titanocene dicarbonyl.

This hydroboration reaction requires elevated temperatures where the reaction mixture is heated to 90°C, the loss of the CO ligand from $Cp_2Ti(CO)_2$ (A) would produce an active site of the coordinately unsaturated $Cp_2Ti(CO)$ complex (B)[83]. Highly reactive species (C), or with the loss of second CO ligand (D) generate the same coordinately unsaturated 16 electron complex (E).[84] The norbornadiene binds to the (E) complex to form (F) followed by a rearrangement of the former Ti (II) complex to Ti(IV) complex (G).[84] Reductive elimination yields exclusively to norbornene-decaborane (NDB) with the Ti (II) complex regenerated to (E). With early transition metal catalyst such as $Cp_2Ti(CO)_2$, the reaction stops after the substitution at B6 boron and does not substitute further at B9 boron of the decaborane moiety. The substituted B6 influences the electronic and chemical properties of the opposites side of the caged cluster, namely B9 boron decreasing its Lewis acidity also known as the antipodal effect.[84]

In this chapter, studies on the various organic-organodecaborane block copolymer syntheses via ROMP using Grubbs 3 catalyst have been conducted. Various compositions of the

monomers in the block copolymer segments were explored and tested to self-assemble into different morphologies.

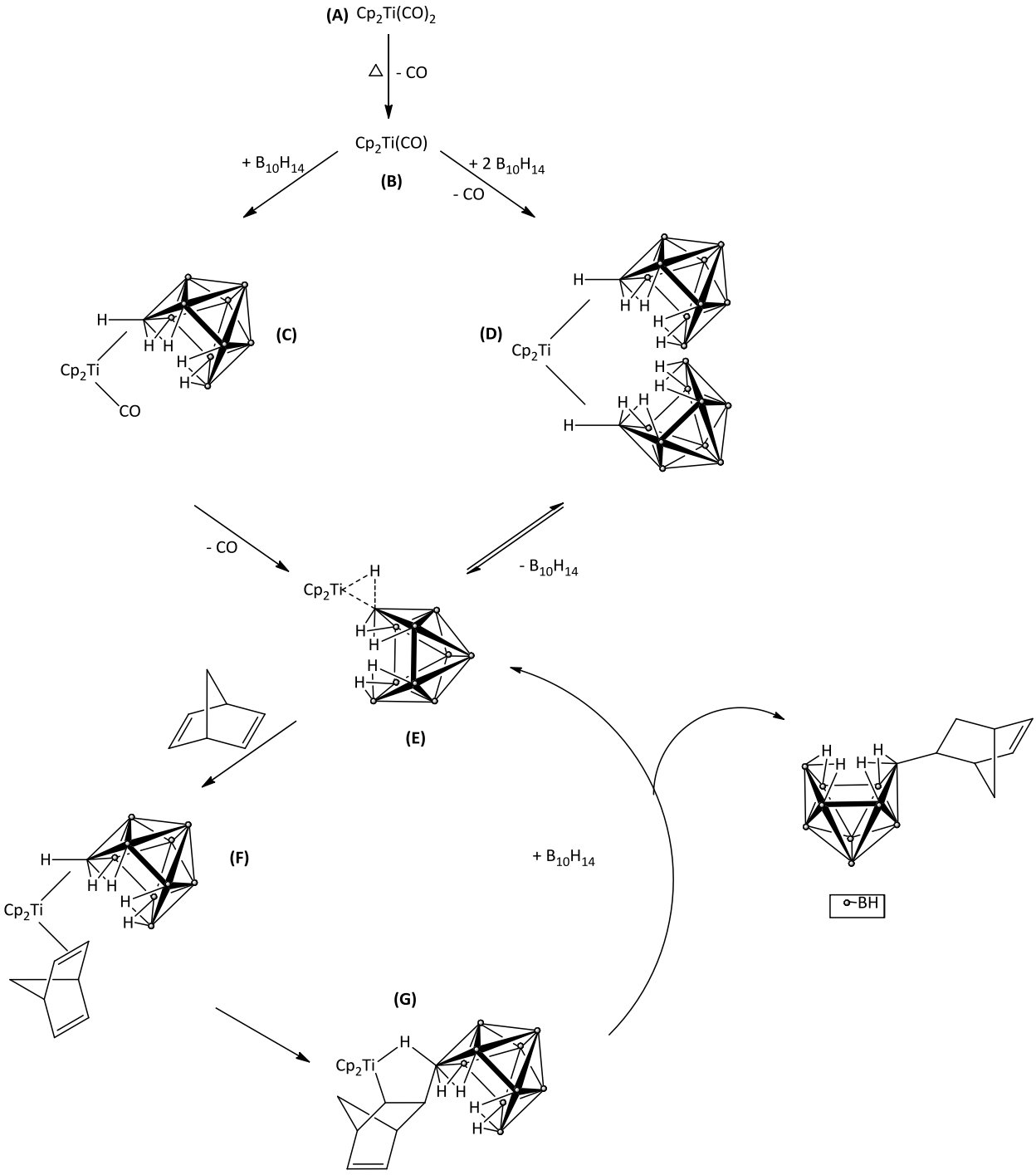

Scheme 3.3- Catalytic process of titanocene dicarbonyl catalyst during hydroboration of decaborane and norbornadiene.

Results and Discussion

MONOMERS

The studies on the hybrid block copolymers were designed around three different monomers. The organic monomers are the parent norbornene (NBE) and the ester functionalized monomer 5- dimethyl cis-5- norbornene-endo-2,3- dicarboxylate (NDC) and NDB as the inorganic monomer. The synthesis of NDB previously shown is a hydroboration reaction of decaborane facilitated by the titanocene dicarbonyl catalyst and excess norbornadiene to yield to 4:1 ratio of exo and *endo* isomer respectively. The hydroboration with the titanium catalyst was limited to one substitution at B6 of the decaborane resulting to only two monosubstitued norbornene isomers. Decaborane has a centre of symmetry where both B6 and B9 carry considerably positive charge and being the most Lewis acidic borons in the molecules. After substitution, the electronic properties of the newly substituted decaborane are comprised influencing the substitution of B9. This is known as the antipodal effect where substitution on one side of the cluster greatly affects the chemical properties as well as the chemical shifts of the borons on the opposite side of the cluster.[85] Therefore, with early transition metal catalysts such as this titanium catalyst, the lowered Lewis acidic B9 cannot take part in the substitution since the stabilization obtained from the back-donation to the B9 would be decreased.[84]

The ^{11}B NMR of norbornenyl-decaborane spectra has a distinct downfield singlet peak near 27.0 ppm belonging to the B6 confirming the hydroboration reaction. The remaining six peaks ranging from 10.0 ppm to -38.0ppm are assigned to B1,3, B9, B8,10 , B5,7 , B2 , and B4

respectively. As mentioned previously, the substitution at the B6 position delocalized the nature of the cluster bonding and influences the chemical shift of the borons on that particular side of the cage. The chemical shifts of B2, B5,7 and B6 have all been shifted downfield from their original chemical shifts in the parent decaborane molecule. In the ^{1}H NMR spectra, there are two olefinic peaks from the *endo* isomer at 6.15ppm and 5.90 ppm whereas the *exo* isomer olefinic peaks are at 6.15 ppm and 6.00 ppm shown in the literature. [82] The terminal BH peaks overlap with the alkyl peaks between 4.0 – 2.50ppm and 1.0-0.0 ppm. The bridged hydrogens have two distinctive peaks far upfield at -1.51ppm from the hydrogens bridged attached to B6 and -2.03 ppm from the hydrogen bridged from B9.

Block copolymers compositions of p(NBE)-*b*-p(NDB) and p(NDC)-*b*-p(NDB) were synthesized. Within these two copolymer families, the chain lengths of 100 and 180 monomer units were synthesized (Table 3.1). Under various temperatures ranging from -40^{o}C to RT, optimal conditions for a linear polymer were tested to achieve controllable polymerization rate to minimize crosslinking.

Table 3.1- Various compositions of the diblock polymer synthesized with Grubbs 3 under various temperatures.

Diblock polymer	Monomer feed (%)						
p(NBE)-*b*-p(NDB)	90/10	80/20	70/30	60/40	50/50	40/60	30/70
p(NDC)-*b*-p(NDB)	90/10	80/20	70/30	60/40	50/50	40/60	30/70

Block copolymers p(NBE)-*b*-p(NDB)

The block copolymers of p(NBE)-*b*-p(NDB) were synthesized using ROMP with Grubbs 3 catalyst under inert atmosphere. For the synthesis of the first block polymer of norbornene, the reaction flask was cooled to -20^{o}C and stirred to 15-35 minutes where the completion was monitored by TLC and NMR. The reaction flasks must be cooled to cryogenic temperatures for controllable and slow the rate of polymerization due to Grubbs 3 high reactivity. In order to ensure proper mixing of the monomer with the catalyst, a concentrated solution of the norbornene monomer in DCM was carefully added to a stirring solution of Grubbs 3 in DCM where the colour changed from green to yellow. The cooling bath was then warmed to -10^{o}C and a concentrated solution of norbornenyl-decaborane in DCM was added and stirred for 15-35 minutes to completion. The reaction was quenched with cold ethyl vinyl ether and warmed to RT (Scheme 3.4). The reaction mixture was exposed and passed through a silica plug to

remove the catalyst. To isolate the polymer, the filtrate is precipitated into vigorously stirring cold pentane followed by centrifuging. The supernatant was discarded and a powdered beige amorphous product was dried under inert atmosphere overnight.

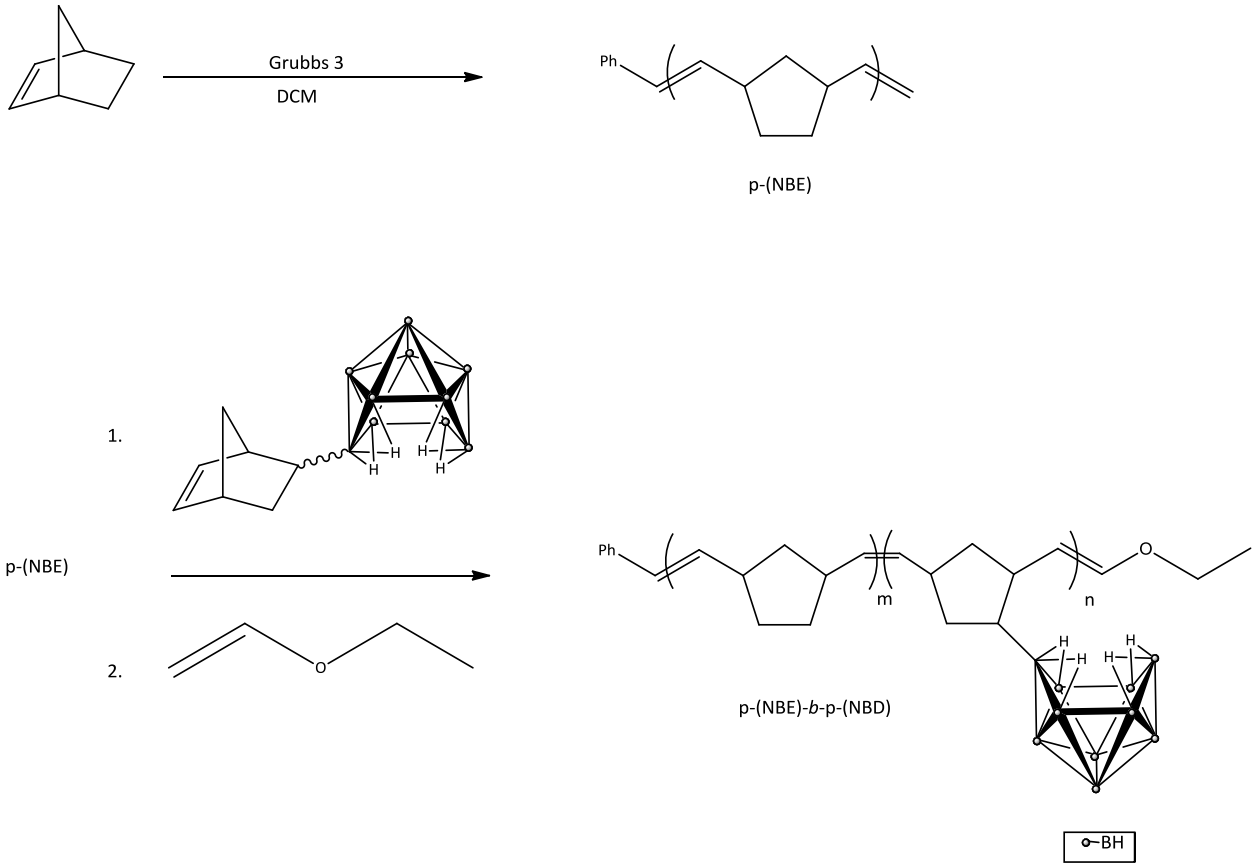

Scheme 3.4- Schematic of the 2-step diblock polymer synthesis. P(norbornene) was first synthesize than without termination of Grubbs 3, a mixture of both norbornenyl-decaborane isomers were added and quenched with ethyl vinyl ether.

Various compositions of both norbornene and norbornenyl-decaborane monomers were synthesized and analyzed in more depth (Table 3.2). The monomer ratio in the feed was calculated to be 70%, 50%, and 30% of p(NDB) in the block copolymer. The monomer units in the block copolymer were determined by ^{1}H NMR to be slightly different than the monomer

feed ratio. The total length of the block copolymers was 180 repeating monomeric units. The time in which the polymerization goes to completion for each block polymer at these specific temperatures increase as the mole fraction increases.

Table 3.2- A concentrated list of the p(NBE)-b-p(NDB) diblock copolymers that were further analyzed showing the actual monomer composition in the polymer and its yields.

Sample	Monomer in the feed (%)		Monomer in the copolymer[1] (%)		Overall weight conversion (%)	Overall molar conversion (%)
	NBE	NDB	NBE	NDB		
1	30.26	69.73	37.07	62.93	81.69	85.63
2	48.03	51.96	53.64	46.35	76.37	79.81
3	69.13	30.86	59.20	40.80	58.78	53.87

[1]Determined by ^{1}H NMR

Proton NMR was a powerful tool used to determine the composition ratio of the block copolymer. The NMRs of p(NBE)-*b*-p(NDB) polymers have broad peaks which are expected with high repeating unit of the monomers. The ^{11}B NMR displays similar peaks pattern of the norbornenyl-decaborane. The peaks from B1, B3, and B9 originally two separate peaks in NDB is one broad in this copolymer as do B5, B7, B8, B10 and B2, B4 (Appendix Figure A3). When

dissolved in the deuterated chloroform-d, the B6 singlet peak is barely visible in the spectra. Yet in deuterated DCM-d2 and deuterated THF-d8 this peak is more apparent. This phenomenon will be discussed in further detail later in the chapter in the self-assembly section. The homopolymers of both norbornene and norbornenyl-decaborane were synthesized using similar conditions as the block copolymer to fingerprint the peaks in the block polymer segment (Figure 3.2). The peaks outline in red represents the BH peaks corresponding to decaboranyl moiety of p(NDB) block with the far upfield BHB bridged hydrogen peaks and the black outline represents peaks belonging to p(NBE) segment. The olefinic region showed overlapped peaks that correspond to both the p(NBE) and p(NDB). This made it difficult to differentiate between the blocks due to the broad multiplets that arise from the different stereochemistry arrangements that exist within the p(NBD) segment. Due to p(NBE) symmetry, the cis and trans are the two dominant tacticity with two distinct peaks around 5.32ppm and 5.19 ppm in the homopolymer spectra. The intensities of the peaks belonging to its' respective block were used to calculate the repeating unit composition percentage of each monomer in the block copolymer. With increasing degree of polymerization of each monomer, the intensity of their corresponding peaks increases and vice versa.

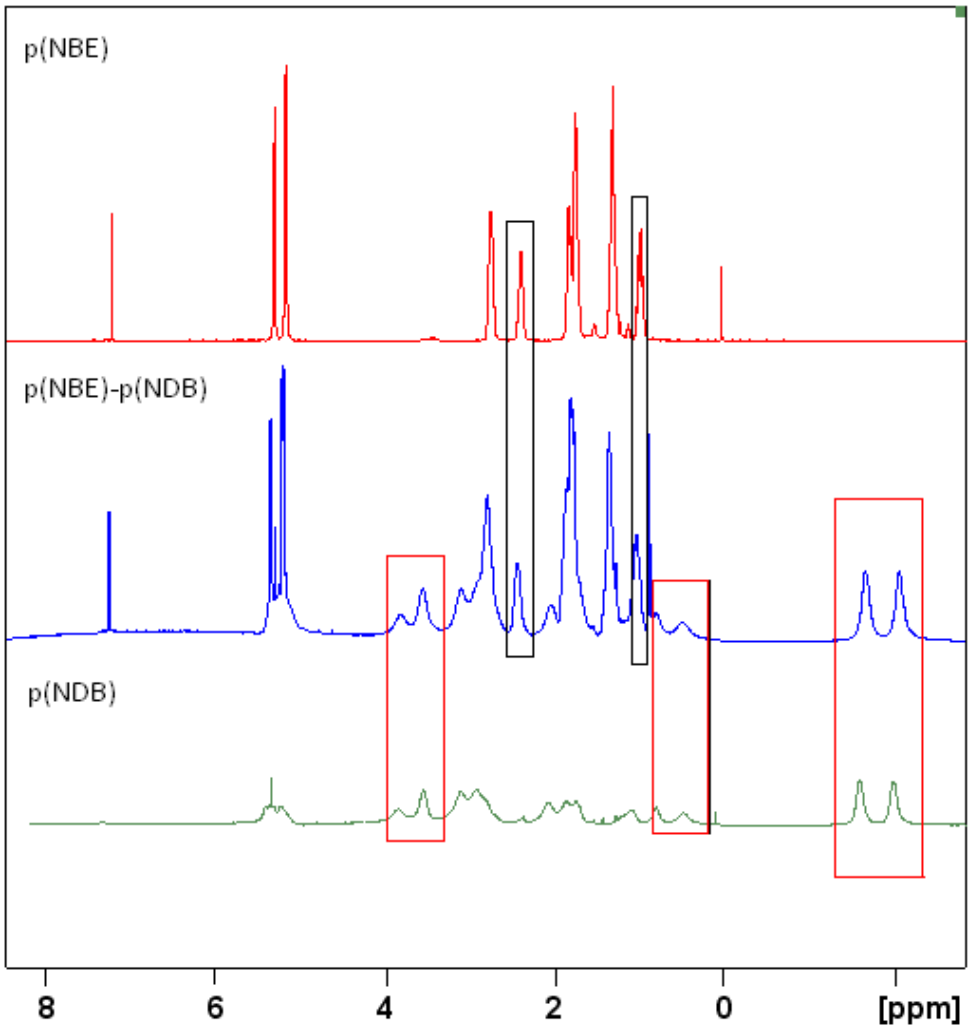

Figure 3.2 – Comparison ^{1}H NMR of $p(NBE)_{60}$-*b*-$p(NDB)_{40}$ block copolymer and the homopolymers of p(NBE) and p(NDB) . The peaks boxed in red represent the peaks exclusive to the p(NDB) block in the block copolymer product. The peaks boxed in black represent the peaks exclusive to the p(NBE) block in the block copolymer product.

A different set of diblock copolymers were synthesized with diester based organic monomer but still maintaining the inorganic NDB monomer. A functionalized norbornene with ester groups were replaced to provide additional stability of the diblock polymer in air and examine its self-assembly abilities with different solvents. The synthesis procedure was performed in a similar fashion as p(NBE)-*b*-p(NDB) copolymers with changes of the cooling baths and the length of time in which monomers were stirred. The 5- dimethyl cis-5- norbornene-endo-2,3-dicarboxylate or (NDC) was dissolved in DCM before transferring to a stirring Grubbs 3 solution at room temperature. The reaction mixture was stirred between 20 to 40 minutes depending on the amount of monomer added (Scheme 3.5). The remainder of the polymerization and workup steps follows the same procedure as the p(NBE)-*b*-p(NDB) copolymers. The final products were off-white powders with yields ranging from 42-91% (Table 3.2). The monomer feed closely agrees with the mole fraction of the monomers incorporated in the diblock copolymers. With the additional ester functional groups on the norbornene, particularly in the *endo* isomer form adds sterics near the double bond slowing the rate of polymerization. As a result, the polymerization was more controlled and cryogenic cooling of the reaction flask is no longer necessary.[80]

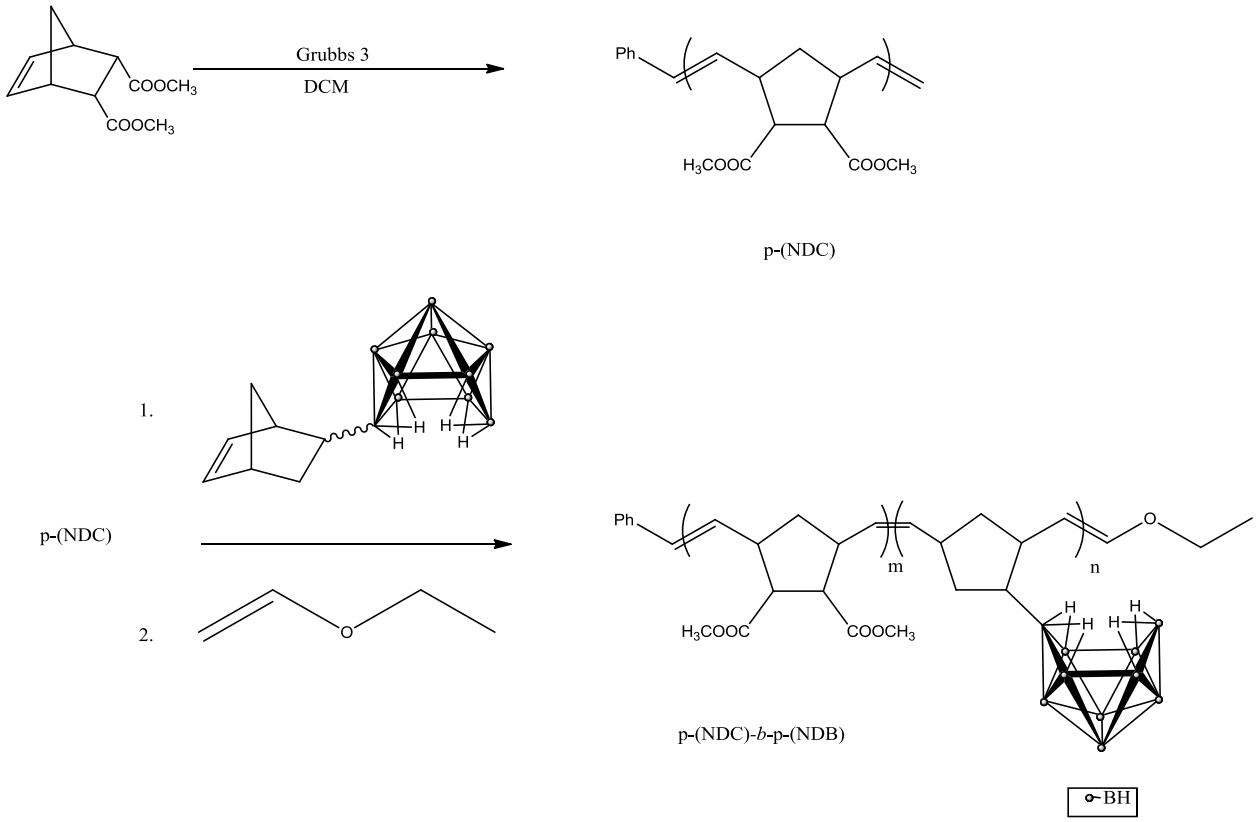

Scheme 3.5- Schematic of the 2-step diblock polymer synthesis. P-(dimethyl cis-5- norbornene-endo-2,3- dicarboxylate) was first synthesize than without termination of Grubbs 3, a mixture of both norbornenyl-decaborane isomers were added and quenched with ethyl vinyl ether.

The ^{1}H NMR spectra consist of broad peaks expected with high degree of polymerization. The olefin peaks belonging to both the monomers overlap at 5.44 ppm in a broad multiplet. With the increase in chiral centers in the organic monomer with ester functional groups, more conformations and tacticity were possible resulting to various olefinic peaks in close range. At 3.63 ppm, a distinct high intensity peak singlet pertaining to the methyl esters followed by broad peaks between 3.60-0.00 ppm from the hydrogens in both blocks. The bridged hydrogen peaks from that decaboranyl moiety remains at the same chemical shifts as seen in p(NBE)-*b*-

p(NDB) copolymers spectra at -1.68 and -2.10 ppm. The peak broadening in the ^{11}B NMR spectra and chemical shifts resemble the p(NBE)-b-p(NDB) copolymers. The broad singlet peak corresponding to B6 is too broad and blends in the shoulder of the B1,B3,B9 peak at about 10 ppm. Two broad singlets at about 0.82 and -3.26 ppm correspond to B5,B7 and B8,B10 respectively. The two broad peak far upfield correspond to the most shielded borons in the cluster at the apex position with B2 at -34.27 ppm and B4 at -38.79 ppm.

Table 3.3- A concentrated list of the p(NDC)-b-p(NDB) diblock copolymers that were further analyzed showing the actual monomer composition in the polymer and its yields.

Sample	Monomer in the feed		Monomer in the copolymer[1]		Overall weight conversion (%)	Overall molar conversion (%)
	NDC	NDB	NDC	NDB		
4	29.89	70.10	35.14	64.86	42.39	42.43
5	50.02	49.97	50.95	49.04	85.23	85.28
6	70.00	29.99	67.63	32.36	91.91	91.86

[1]Determined by ^{1}H NMR

GPC

GPC using UV and DRI detectors was used to determine the Mn, Mw and PDI of the polymers. The homopolymers of p(NDC)and p(NDB) were analyzed as benchmarks for the process and for comparison. The measurements on these species reached PDIs as low as 1.08. Attempts on aquiring acceptable data of the block copolymers with these detectors were not successful. These measurements yielded only very broad peaks with PDIs as large as 6.00. This is no surprise since the HPLC THF solvent was used the block copolymers aggregrate into micelles causing inaccurate molecular weight readings. Multidetector system that include detectors UV and DRI paired molecular weight sensitive detectors such as MALLS or LALLS would provide more accurate readings of the Mn and Mw of block polymers and better PDI readings.

THERMAL ANALYSIS – TGA/DSC

TGA analysis of $p(NBE)_{70}$ -*b*-$p(NDB)_{30}$ was reported by Malenfant *et al*.[8] TGA analysis were conducted and showed decomposition at 242^{o}C that is the crosslinking and decomposition of the decaboranyl moieties.[8] A second decomposition at 400^{o}C occurred due to the decomposed carbon backbone.[8] TGA analysis was conducted on a p(NDC)-*b*-p(NDB) copolymer under nitrogen atmosphere and showed a two-step decomposition at 149^{o}C and at 232^{o}C, followed by a second weight loss at 403^{o}C (Figure 3.3). The initial decomposition marks the decomposition and crosslinking to the decaboranyl moities.[8, 82, 86] At 403^{o}C, the weight loss

was attributed to the decomposition of the carbon backbone of the polymer. A weight increase occurs at 742°C, followed by a steady decrease weight loss to 1000°C. .

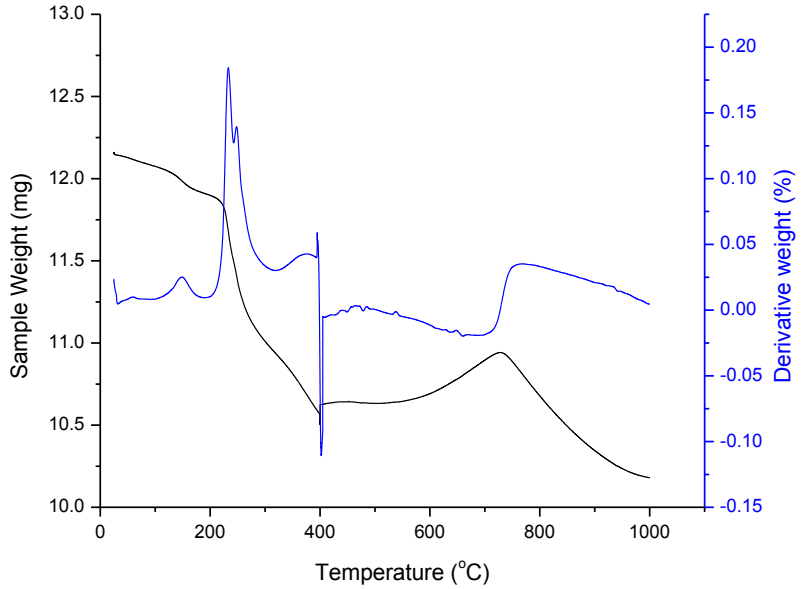

Figure 3.3- TGA/DTA analysis of p(NDC)-*b*-p(NDB). From RT to 400°C a ramp of 10°C/min was applied and dwelled for 20 mins continued at a ramp of 10°C/min to 1000 °C.

DSC analyses were initially carried out with the homopolymers at a ramp cycle of 10°C/min under nitrogen atmosphere to acquire information about their transitions. The melting temperature (T_m) peak of the p(NDB), p(NDC) and p(NBE) polymers were 300-450°C, 400-500 °C, and 400-500 °C respectively. The glass transition temperature (T_g) of the p(NBE) was found to be 62°C, which is slightly higher than the 30-40 °C reported in the literature.[87] Since these are kinetic transitions, the heating rate has an effect on the T_g. The T_g of both p(NDC) and p(NDB) homopolymers were less prominent as they were overlapped by exothermic peaks at 75 °C and 96°C respectively.

The block copolymers at a ramp cycle of 10^{o}C/min under nitrogen atmosphere. The melting temperature (T_m) peak of the p(NBE)-b-p(NDB) polymers range between 250- 400^{o}C(Figure 3.4 A and B). The DSCs of p(NDC)-b-p(NDB) showed similar curve patterns with the T_m range between 315- 425^{o}C (Figure 3.4 C and D). Both sets of diblock copolymers showed two sets of exothermic peaks between 100^{o}C-140^{o}C and 250^{o}C to 285^{o}C. With the polymers stored below the T_g for prolong periods of time, the polymers experience decrease molecular mobility and increase in brittleness. Therefore they were not at thermodynamical equilibrium and their chemical unstability resulted in crystallization of the polymer. In attempts to counteract these effects and get cleaner DSC plots, the polymers were subjected to a second round of heating with different ramp cycles. The polymers were rapidly heated to 150^{o}C, followed by slow cooling ramp of 2^{o}C/min to RT, reheated at the same rate to 150^{o}C and finally heating to 550^{o}C at a faster ramp of 5^{o}C/min (Figure 3.4 E and F). Upon second heating, the polymer's exothermic peaks between 100-140^{o}C were significantly reduced but the prominent exothermic peaks between 258-261^{o}C remained as it indicates crosslinking of the polymer. This was evident has through the cooling segment where no T_g's appeared. Since these polymers are block copolymer, two T_g's could appear on the DSC curve. Though, the majority of the diblock copolymers showed one T_g peak that corresponds to the p(NDB) block. The T_g of the polymers seem to be near or overlap with the first exothermic peak ranging between 70-80^{o}C and 85-95^{o}C for the p(NBE)-b-p(NDB) and p(NDC)-b-p(NDB) respectively.

A)

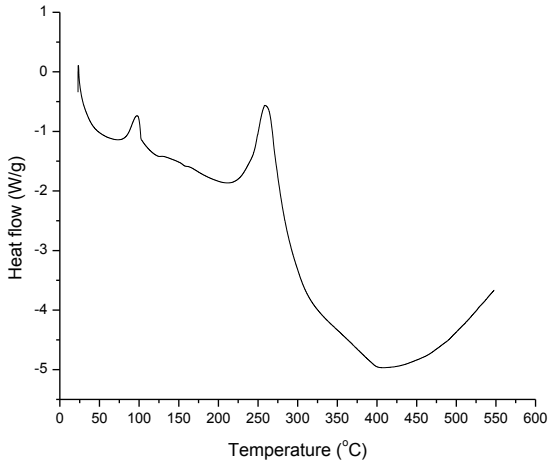
Heat flow (W/g)
Temperature (°C)

B)

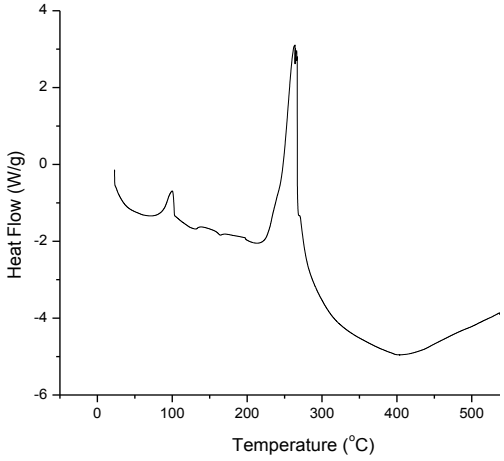
Heat Flow (W/g)
Temperature (°C)

C)

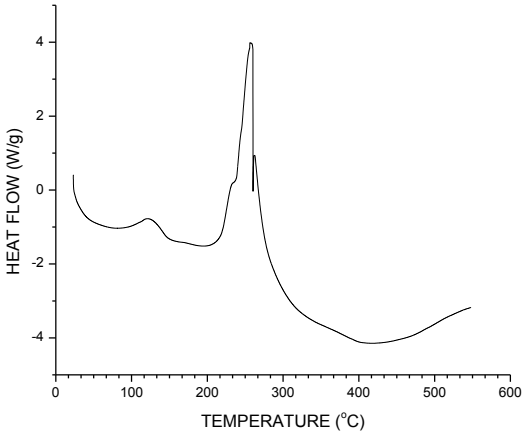
HEAT FLOW (W/g)
TEMPERATURE (°C)

D)

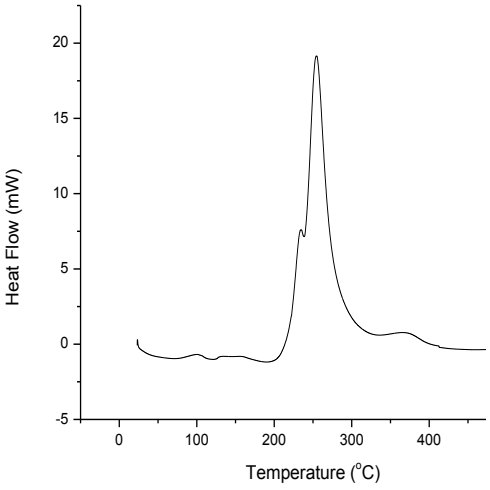
Heat Flow (mW)
Temperature (°C)

E)

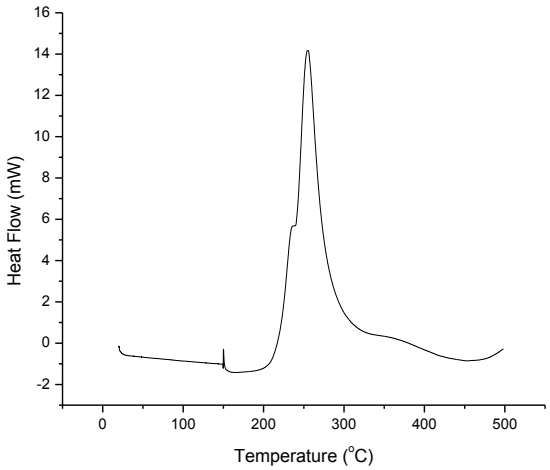

F)

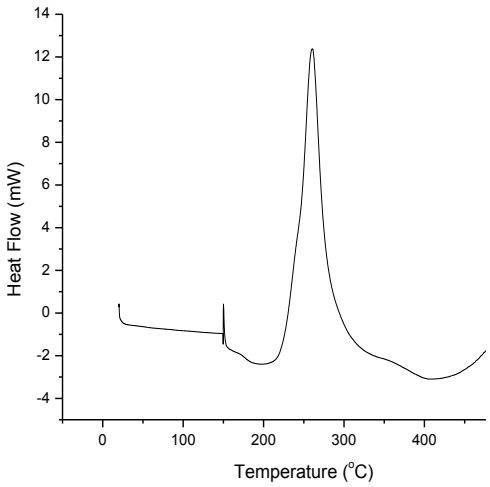

Figure 3.4- DSC analysis of the block copolymers. DSC curves at ramp of 10°C/min from RT to 550°C for (A) $p(NBE)_{70}$-*b*-$p(NDB)_{30}$, (B) $p(NBE)_{60}$-*b*-$p(NDB)_{40}$, (C) $p(NDC)_{30}$-*b*-$p(NDB)_{70}$, and (D) $p(NDC)_{40}$-*b*-$p(NDB)_{60}$ .Different ramp cycle for (E) $p(NDC)_{70}$-*b*-$p(NDB)_{30}$ and (F) $p(NBE)_{50}$-*b*-$p(NDB)_{50}$ that have undergone second heating starting at RT to 150°C at 2°C/min followed by a ramp of 5°C/min to 550°C.

In order to investigate the self-assembled structures of the diblock copolymers, the block copolymers were dried via slow solvent evaporation anticipating effects that would arising from both the nature of the solvent and the relative block structures of the copolymers. The diblock copolymers were dissolved in various dry solvents in 1mg/mL solutions and their morphologies were observed via SEM. Self-assembly was achieved by slow solvent evaporation where the solvent evaporates, micelles are formed with the majority of diblock copolymers showing disordered cylindrical domains when dissolved in DCM, toluene, and chloroform as $p(NBE)_{53}$-*b*-$p(NDB)_{47}$ (Figure 3.5 A, B and C). The diblock copolymers of $p(NDC)_{70}$-*b*-$p(NDB)_{30}$ did not display any morphology patterns in the SEM images where polymers experienced macrophase separation (Figure 3.5 D).

The SEM image of p(NBE)$_{59}$-*b*-p(NDB)$_{41}$ revealed that the polymers dissolved in chloroform form lamellar morphology (Figure 3.5 E). The slight curves of the lamellae structures could be the result of crosslinking which indicates that the polymer is not completely uniform. On the other hand, when this polymer evaporates from THF, disordered micelles were form where the micelles vary in size (Figure 3.5 F). This composition may not satisfy the mole fraction required to form the cylindrical domains. The lamellar morphology was achieved since is it least difficult to form as the theoretical AB diblock phase morphology shown in chapter 1 (Figure 1.4) as it can be accomplished with wider range of the volume fraction of the monomers.

Malenfant *et al.* had previously synthesized p(NBE)$_{70}$-*b*-p(NDB)$_{30}$ polymers that satisfy the Flory-Huggins interaction parameter and acquired ordered cylindrical and lamellar morphology using THF and chloroform respectively (Figure 3.6). In the cylindrical morphology, the THF surrounds the decaboranyl moieties resulting in packed hexagonal cylinder with the hydrophobic p(NBE) blocks are retained in the core. Elemental mapping confirmed that he darker layers represents the p(NBE) block and p(NDB) the lighter layers[8].

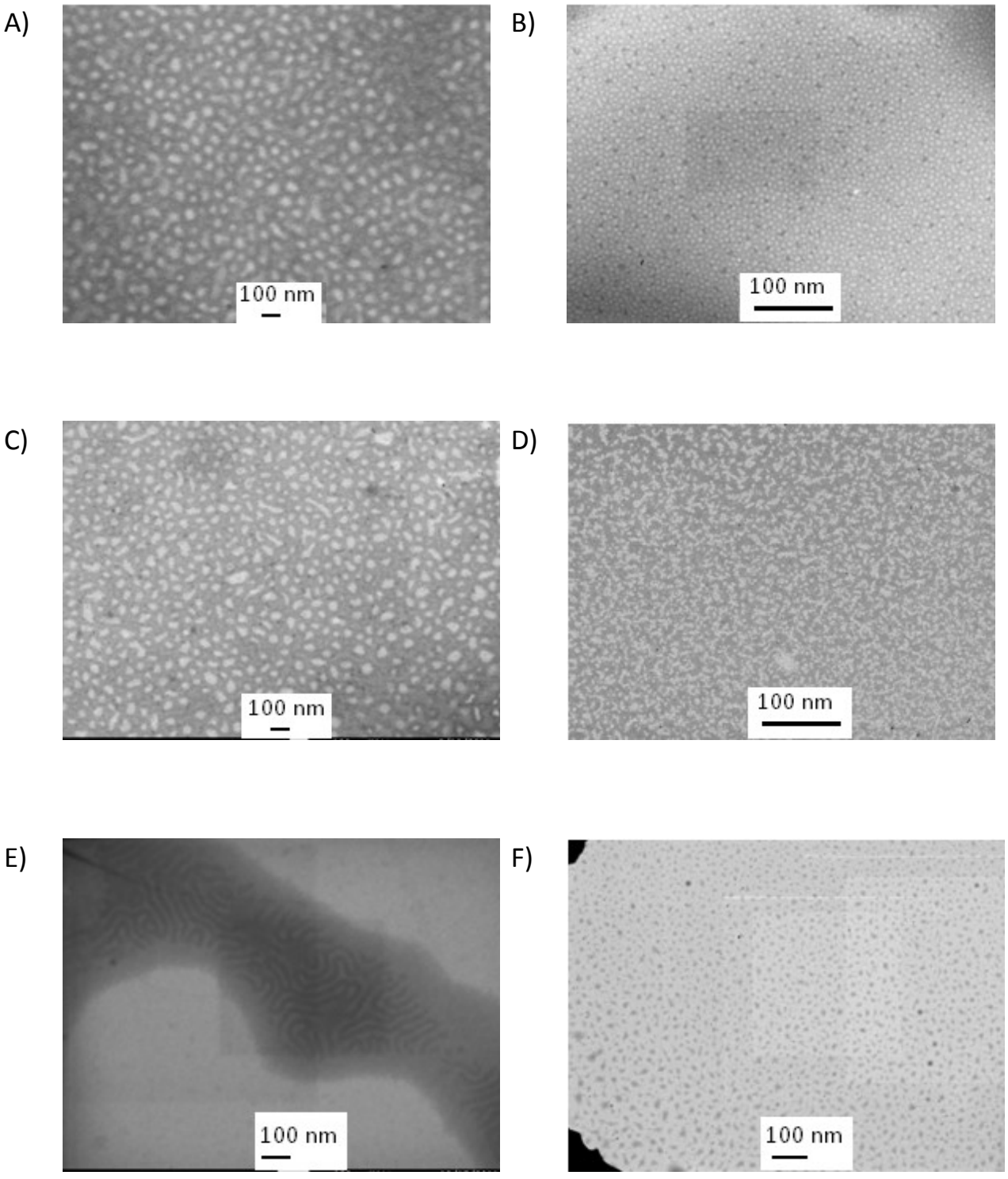

Figure 3.5- SEM images block copolymers after evaporation. (A) $p(NBE)_{50}$-b-$p(NDB)_{50}$ after evaporation in toluene; (B) p(NBE)50-b-p(NDB)50 after evaporation in DCM; (C) p(NBE)50-b-p(NDB)50 after evaporation in chloroform; (D) $p(NDC)_{70}$-b-$p(NDB)_{30}$ after evaporation in chloroform; (E) $p(NBE)_{60}$-b-$p(NDB)_{40}$ after evaporation in chloroform; (F) $p(NBE)_{60}$-b-$p(NDB)_{40}$ after evaporation in THF

A)

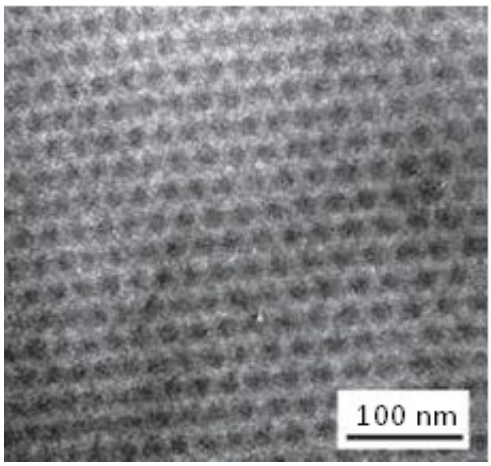

B)

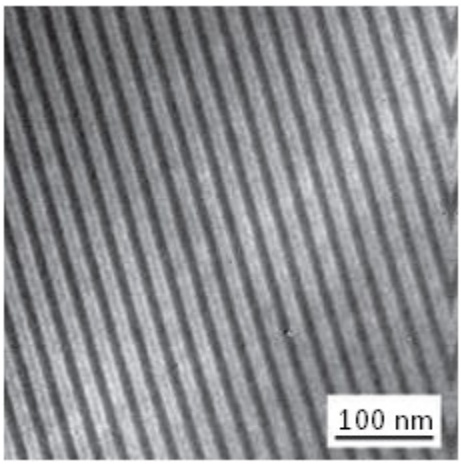

Figure 3.6 [8]-TEM images on $p(NBE)_{70}$-*b*-$p(NDB)_{30}$ after slow solvent evaporation in THF (A) and in Chloroform (B).

Experimental

6-(5-Norbornenyl)-decaborane

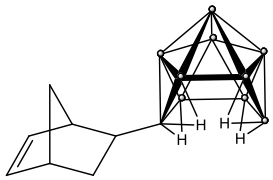

Exo

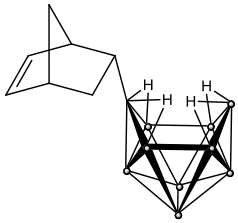

Endo

Decaborane (6.05g, 49.50 mmol) and 3 mol % of titanocene dicarbonyl (0.405g, 1.73 mmol) were dissolved in dry 2,5-norbornadiene solution (30mL, 301.00 mmol) in a 100mL Schlenk tube equipped with a magnetic stirring bar under nitrogen atmosphere. The reactants were stirred to homogeneity before sealing the Schlenk and then transferred to a fumehood. The reaction mixture was heated in a 90^{o}C oil bath for 96 hr. A colour change from brown to dark green was observed within the first 1 h. The Schlenk tube seal was removed, and the reaction mixture was stirred and exposed to air for an additional 10 minutes. The reaction mixture was concentrated before passing through a column chromatography washed with hexanes. The fractions were combined and the hexanes was removed via rotovap and dried under vacuum to afford off-white powder with 82% yield. The crude product was purified by recrystallization in toluene at RT and stored in the fridge for 48 hr to afford colourless crystals (exo-2,5-norbornenyldecaborane) and a pale yellow oil.

Exo-isomer

^{11}B NMR (500 MHz, $CDCl_3$) δ 28.2 (s, 1H, B6), 10.3 (d, 2H, B1,3, J= 146 Hz), 8.80 (s, 1H, B9), 1.42 (d, 2H, B5,7, J= 148 Hz), -3.05 (d, 2H, B8,10, J= 146 Hz), -33.6 (d, 1H, B2, J= 154 Hz), -38.4 (d, 1H, B4, J=154 Hz),

^{1}H [^{11}B] NMR (500 MHz, $CDCl_3$) δ 6.15 (dd, 1H, J= 9.15 Hz, J= 505 Hz), 6.00 (dd, 1H, J= 10.05 Hz, J= 5.95 Hz), 3.83 (br s, 1H), 3.53 (br s, 2H), 3.10 (br s, 2H), 2.96 (s, 1H), 2.94 (s, 1H) 2.89 (br s, 1H), 1.73 (dd, 1H, J= 8.75 Hz, J= 5.7 Hz), 1.69 (dd, 1H, J= 8.4 Hz, J= 6.1 Hz), 1.41 (m, 1H), 1.34 (d, 2H, J= 2.65 Hz), 1.25 (m, 1H), 0.84 (br s, 1H, BH), 0.47 (br s, 1H, BH), -1.51 (br s, 2H, BHB), -2.03 (br s, 2H, BHB)

^{13}C NMR (500 MHz, $CDCl_3$) δ 137.6, 135.6, 47.7, 46.8, 42.9, 32.4

Endo-isomer

^{11}B NMR (500 MHz, $CDCl_3$) δ 27.7 (s, 1H, B6), 9.65 (d, 2H, B1,3, J=146 Hz), 8.23 (d, 1H, B9, J=162 Hz),0.98 (d, 2H, B5,7, J=156 Hz), -3.21 (t, 2H, B8,10, J=131 Hz), -33.8 (d, 1H, B2, J= 154 Hz), -38.9 (d, 1H, B4, J= 156 Hz),

^{1}H[^{11}B] NMR (500 MHz, $CDCl_3$) δ 6.14 (dd, 1H, J= 5.65 Hz, J= 3.10 Hz), 5.89 (dd, 1H, J= 6.55 Hz, J= 3.50 Hz), 3.79 (d, 1H, J= 6.60 Hz), 3.51 (br s, 2H), 3.09 (br s, 2H), 3.04 (br s, 1H), 2.92 (br s, 1H), 2.79 (d, 2H, J= 18.35 Hz), 2.15 (td, 1H, J=9.7 Hz, J= 3.7 Hz), 2.04 (m, 1H), 1.46 (dd, 1H, J=8.1 Hz, J=1.7 Hz), 1.42 (s,2H), 1.25 (d, 1H, J= 6.55 Hz), 1.12 (ddd, 1H, J=11.35 Hz, J= 4.85 Hz, J=1.95 Hz), δ -1.51 (br s, 2H, BHB), δ -2.03 (br s, 2H, BHB)

^{13}C NMR (500 MHz, $CDCl_3$) δ 138.3, 133.1, 51.2, 47.1, 43.0, 32.8

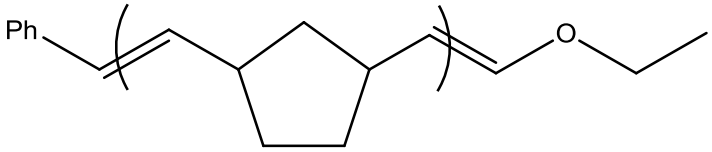

Poly(norbornene) or p(NBE)

Grubbs 3 catalyst and norbornene were dissolved separately in DCM in round bottom flasks equipped with magnetic stirring bar under inert atmosphere. The flasks were sealed with septum caps and placed in acetonitrile/dry ice cooling bath (-20^{o}C) where the solutions stirred for 10 minutes. The norbornene solution was transferred to the Grubbs 3 solution carefully via cannula transfer and stirred for 30 minutes where the colour change from green to orange was observed. The reaction was quenched with cold ethyl vinyl ether and the reaction mixture was allowed to warm up to RT for 15 minutes. The reaction mixture was exposed to air and quickly washed and through a silica plug with DCM to remove the catalyst. The filtrate was concentrated via rotovap and precipitated in cold pentane. The mixture was centrifuged, the supernatant discarded and the white precipitate was slowly dried under inert atmosphere resulting to a white powder.

^{1}H NMR (500 MHz, $CDCl_3$) δ 5.32 (br s, 1H, trans), 5.19 (br s, 1H, cis), 2.77 (br s, 1H, cis), 2.41 (br s, 1H, cis), 1.85 (q, 1H, J= 5.85 Hz), 1.78 (d, 2H, J=4.35 Hz), 1.33 (br m, 2H), 1.02 (m, 1H)

^{13}C NMR (500 MHz, $CDCl_3$) δ 133.8, 133.0, 43.4, 43.1, 42.7, 42.0, 41.3, 38.6, 38.4, 33.1, 32.9, 32.3, 32.1

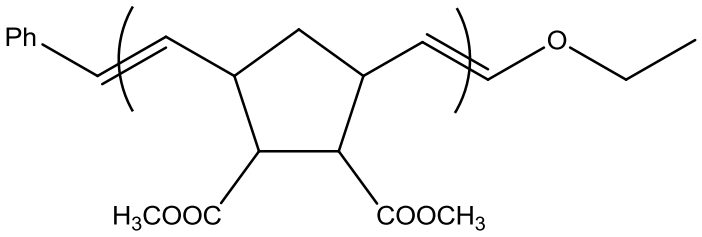

Poly (dimethyl cis-5- norbornene-endo-2,3- dicarboxylate) or p(NDC)

Grubbs 3 catalyst and NDC were dissolved separately in DCM in a round bottom flasks equipped with magnetic stirring bar under inert atmosphere. The NDC solution was transferred into the catalyst solution via a syringe and the reaction mixture was stirred to completion where the colour change from green to greenish/brown was observed. The reaction was quenched with cold ethyl vinyl ether and stirred for an additional 15 minutes where the colour change from greenish/brown to orange was observed. The reaction flask was exposed to air and quickly washed and filtered through a silica plug with DCM to remove the catalyst. The filtrate was concentrated via rotovap and precipitated in cold methanol. The white precipitate was isolated

by centrifuge where the supernatant was discarded and dried under vacuum to afford a white powder.

^{1}H NMR (500 MHz, $CDCl_3$) δ 5.50 (br m, 2H), 3.63 (br m, 6H), 3.11 (br m, 3H), 2.83 (br m, 1H), 1.90 (br m, 2H)

^{13}C NMR (500 MHz, $CDCl_3$) δ 172.9, 172.4, 134.9, 51.54, 51.38, 48.71, 48.10, 46.28, 39.11

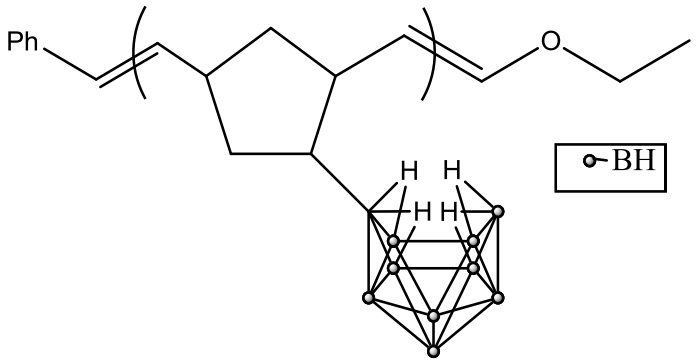

Poly(norbornenyl-decaborane) or p(NDB)

Grubbs 3 catalyst and NDB were dissolved separately in DCM in ~~a~~ round bottom flasks equipped with magnetic stirring bar under inert atmosphere. The flasks were sealed with septum caps and placed in acetonitrile/dry ice cooling bath (-10^{o}C) where the solutions stirred for 10 minutes. The NDB solution was transferred to Grubbs 3 solution carefully via cannula transfer and stirred to completion where the colour change from green to orange was observed. The reaction was quenched with cold ethyl vinyl ether and the reaction mixture was allowed to

warm up to RT for 15 minutes. The reaction flask was exposed to air and quickly filtered and washed through a silica plug with DCM to remove the catalyst. The filtrate was concentrated via rotovap and precipitated in cold pentane. The mixture was centrifuged and the supernatant discarded and precipitate was slowly dried under inert atmosphere resulting to a beige/tan powder.

^{11}B NMR (500 MHz, CD_2Cl_2) δ 26.4 (s, 1H, B6), 9.99 (s, B1, 3, 9), 0.63 (br s, 2H, B8, 10), -3.20 (br s, 2H, B5, 7), -34.4 (d, 1H, B2), -38.4 (br s, 1H, B4)

^{1}H[^{11}B] NMR (300 MHz, CD_2Cl_2)δ 5.33 (m, 2H), 3.85 (br s, 2H, BH), 3.57 (br s, 1H, BH), 3.03 (d, 3H, J= 58.74 Hz, BH), 2.27 (br s, 2H), 1.81 (d, 4H, J= 35 Hz, BH), 1.11 (br s, 1H), 0.82 (br s, 1H), 0.50 (br s, 1H), -1.58 (br s, 2H, BHB), -1.98 (br s, 2H, BHB)

^{13}C NMR (300 MHz, CD_2Cl_2) δ 136.2, 134.0, 132.0, 45.8, 43.6, 42.4, 40.0, 37.6, 35.4

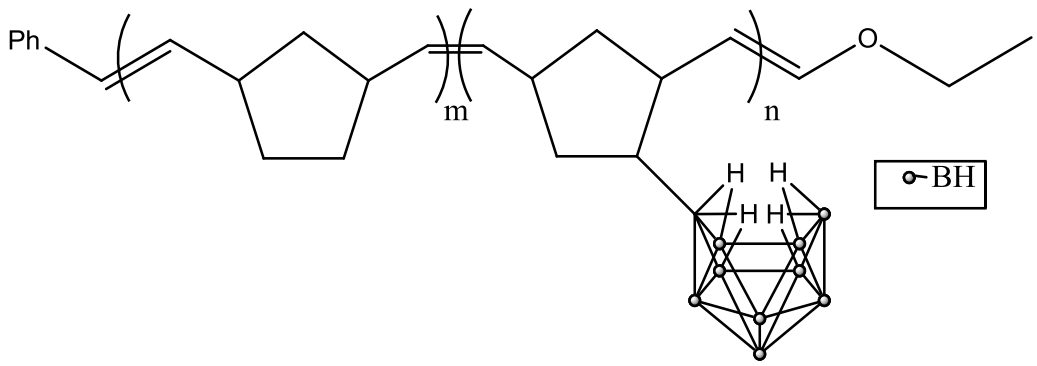

Poly(norbornene)-*b*- poly(norbornenyl-decaborane) or p(NBE)-*b*-p(NDB)

Grubbs 3 catalyst and norbornene were dissolved separately in DCM in round bottom flasks equipped with magnetic stirring bar under inert atmosphere. The flasks were sealed with septum caps and placed in acetonitrile/dry ice cooling bath (-20^{o}C) where the solutions stirred for 10 minutes. The norbornene solution was transferred to Grubbs 3 solution carefully via cannula transfer and stirred to completion where the colour change from green to orange was observed. The reaction mixture was warmed to -10^{o}C. NDB was dissolved separately in DCM in round bottom flasks equipped with magnetic stirring bar under inert atmosphere and sealed was septum cap. The flask was cooled to -10^{o}C prior to transferring the NDB solution via cannula to the reaction mixture. The reaction was stirred to completion (the length of time varies with the amount of monomers added to the reaction mixture) and quenched with cold ethyl vinyl ether. The reaction mixture was stirred for 15 minutes and allowed to warm up to RT. The reaction mixture was exposed to air and quickly washed through a silica plug with DCM

to remove the catalyst. The filtrate was concentrated via rotovap and precipitated in cold pentane. The mixture was centrifuged and the supernatant discarded and the precipitate was slowly dried under inert atmosphere resulting to a beige/tan powder and is stored in the glovebox.

$^{11}B[^{1}H]$ NMR (300 MHz, $CDCl_3$) δ 10.65, 2.63, -34.17, -38.47

$^{1}H[^{11}B]$ NMR (300 MHz, $CDCl_3$) δ 5.37 (m, 2H), 5.22 (d, 2H, J= 5.94 Hz), 3.87 (br s, 1H), 3.57 (br s, 1H), 3.12 (br s, 1H), 2.81 (br s, 4H), 2.47 (br s, 1H), 2.08(br s, 1H), 1.82 (m , 6H), 1.37 (m, 3H), 1.04 (m, 2H), 0.94 (m, 1H), 0.51 (br s, 1H), -1.65 (br s, 2H, BHB), -2.06 (br s, 2H, BHB)

^{13}C NMR (300 MHz, $CDCl_3$) δ133.9, 133.0, 43.4, 43.1, 42.7, 42.1, 41.4, 38.7, 38.4, 33.1, 32.9, 32.3, 32.2,

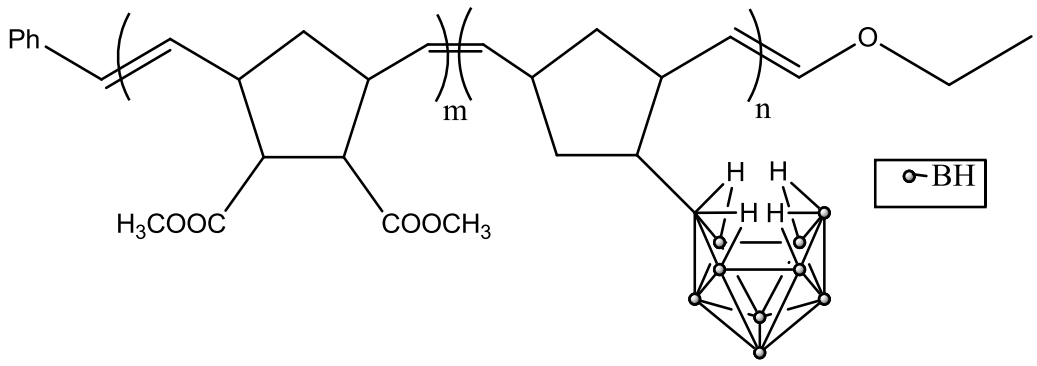

Poly (dimethyl cis-5- norbornene-endo-2,3- dicarboxylate) -*b*- poly(norbornenyl-decaborane) p(NDC)-*b*-p(NDB)

Grubbs 3 catalyst and NDC were dissolved separately in DCM in round bottom flasks equipped with magnetic stirring bar under inert atmosphere. The NDC solution was transferred into the catalyst solution via a syringe and the reaction mixture was stirred to completion at RT where the colour change from green to greenish/brown was observed. The reaction flask was sealed with a septum caps placed in a cooling bath (acetonitrile/dry ice) to -10^{o}C. NDB was dissolved separately in DCM in round bottom flasks equipped with magnetic stirring bar under inert atmosphere and sealed with a septum cap. The flask was cooled to -10^{o}C prior to transferring the NDB solution via cannula to the reaction mixture. The reaction was stirred to completion and quenched with cold ethyl vinyl ether. The reaction mixture was stirred for 15 minutes and allowed to warm up to RT. The reaction mixture was exposed to air and quickly washed through a silica plug with DCM to remove the catalyst. The filtrate was concentrated via rotovap and

precipitated in cold pentane. The mixture was centrifuged and the supernatant discarded and the precipitate was slowly dried under inert atmosphere resulting to a beige/tan powder and is stored in the glovebox.

$^{11}B[^{1}H]$ NMR (500 MHz, $CDCl_3$) δ 25.10, 10.31, 0.82, -3.26, -34.27, -38.79

$^{1}H[^{11}B]$ NMR (500 MHz, $CDCl_3$) δ 5.44 (br m, 4H), 3.63 (br s, 6H), 3.59 (br s, 2H), 3.10 (br s, 5H), 2.84 (br s, 3H), 1.91 (br m, 4H), 1.68 (br s, 1H), 1.40-0.28 (5H, BH), – 1.68 (br s, 2H), -2.10 (br s, 2H)

^{13}C NMR (500 MHz, $CDCl_3$) δ 172.9, 134.9, 51.5, 51.3, 48.7, 48.1, 46.3, 39.1

Chapter 4: Boron Nitride and Boron Carbonitride Ceramics

Introduction

There is a recent and growing interest in inorganic non-oxide ordered mesoporous materials due to their broad functional properties in various fields. The initial downfall of the lack of controllable sol-gel processes for non-oxide materials has been alleviated by the improvements in the synthesis of non-oxide mesoporous materials via inorganic polymer precursors; organic-organic cooperative assemblies; nanocasting; and *in situ* post-transformation from solid-gas reactions. [11b, 88]

The goal for these mesoporous materials is the preparation of materials with uniform pore size ranging between 2-50nm in an orderly fashion throughout the ceramic. With the advantage of creating tunable pore sizes, reaction/interaction sites on the ceramic can utilize the high surface areas for processes such as catalysis, electrochemistry applications and sorption.[89] These void spaces from the pores can accommodate larger molecules than conventional micropores to be embedded within the ceramic for catalysis, adsorption, separation, and drug delivery purposes.[88a]

Boron nitride (BN) possess isostructural and isoelectronical similarities to the carbon lattice where various crystalline forms can be obtained.[90] The most stable form include the graphitic phase, α-BN or hexagonal-BN, where an alternate arrangement of covalent boron and nitrogen bonds in six-membered rings joined in two dimensional layers forming a hexagonal unit (Figure 4.1 A).[91] The BN bonds are sp^2 hybridized with the layer stacked in AB sequence where the

atoms in the layer lay directly above or below are of the opposite atom and binds via weak Van Der Waals interactions.[91] The cubic-BN or β-BN, is a dense BN with isostructural similarities to diamond.[92] This differs from the α-BN where the BN bonds are sp^3 hybridized with sphalerite structure (Figure 4.1 B).[91] The cubic β-BN can be synthesized from h-BN subjected to high temperatures and pressure.[93] Other forms such as rhombohedral BN, resembling α-BN with the a three-layers stacking sequence ABC that can be converted to β-BN as well.[94] A rare h-BN form with a wurtzite structure also exists with boron and nitrogen bonded in a tetrahedral configuration.[95] And finally, there are two kinds of disordered BN phases that include turbostratic that is similar to h-BN with the difference that the layers are parallel and not aligned to the c-axis, and amorphous.[95-96]

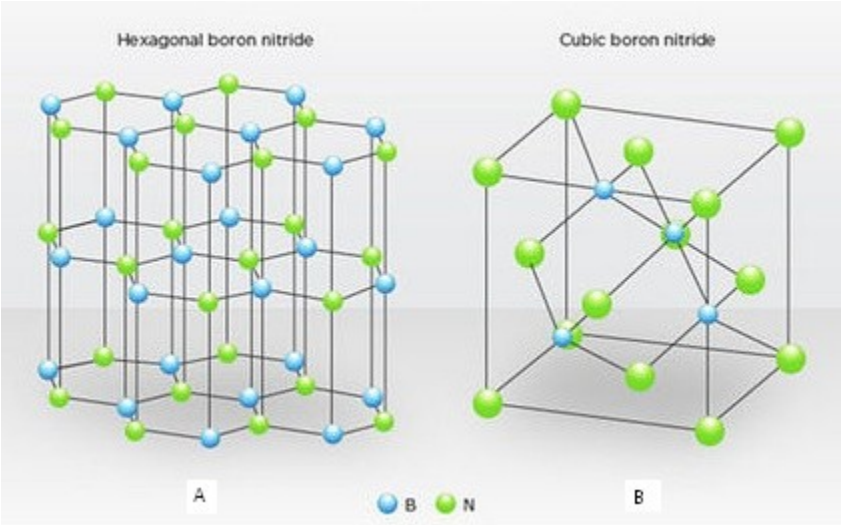

Figure 4.1 [9]- Diagrams of the most stable forms of BN. (A) α-BN or hexagonal-BN, (B) β-BN or cubic-BN.

Hexagonal BN is traditionally prepared by heating a boron and nitrogen source to high temperatures.[93] Using boron oxide, elemental boron, metal borides, boron halides, and

borohydrides heated under ammonia or nitrogen atmosphere are amongst the common precursors used to synthesize BN.[91]

Most polymeric precursors of BN have been derived from borazines or boranes molecules. Borazine is an inorganic compound that is isoelectronic and isostructural to benzene with a chemical formula of $(BH)_3(NH)_3$. Borazine and its derivatives have been pyrolyzed under pressure, a condition required due to its low boiling point.[97] The borazine compounds undergo condensation producing analogues of naphthalenes and biphenyl structures that further crosslinks into BN.[97] Alternative borazine polymers include are aminosubstituted borazines, such as $[(CH_3)_2NBNH]_3$, that undergo ammonolysis when heated to 1200^{o}C, to produce a pure inorganic aminosubstituted borazine precursor for a highly pure BN.[91]

Boranes are another class of compounds used in preparation of polymers that can further be converted in BN. This classification can be subdivided into two routes[91]:

1) Reactions of bifunctional amines or ammonia with boranes as a polymer preparation or;
2) Boranes functionalized with unsaturated organic groups to form polymers.

Borane provides the boron needed to create BN since the polymers primarily contain carbon and are deficient in nitrogen, the polymers undergo pyrolysis under a stream of ammonia gas to produce BN.[86] The earliest reaction includes diborane adduct $B_2H_6{\cdot}2NH_3$ pyrolyzed between 900-1500^{o}C to generate BN.[91] A synthesis of poly(vinylpentaborane) and pyrolyzed to produce hexagonal BN at 1450^{o}C under ammonia atmosphere were reported in the late 1980's (Scheme 4.1) .[10] Upon pyrolysis, the polymer forms an intermediate where the pentaboranyl moieties form borazanaphthalene units with the release of hydrogen gas as a byproduct before forming

BN.[98] Nitrogen source was introduced in the reaction while heating via ammonia gas as a result the polymer experiences a net weight gain.

Decaborane, a compound of the borohydride family, has also been used to make BN. A simple direct procedure involves decaborane and ammonia to produce $B_{10}H_{12}{\cdot}2NH_3$ intermediates followed by formation of BN at temperatures between 800-1180°C. [99] An alternative route began with decaborane reacting with bifunctional amines to produce a polymer, $[B_{10}H_{12}N(H_2)CH_2CH_2N(H_2)]_X$, that was then pyrolyzed to 1000°C under ammonia atmosphere to produce pure white BN. [100]

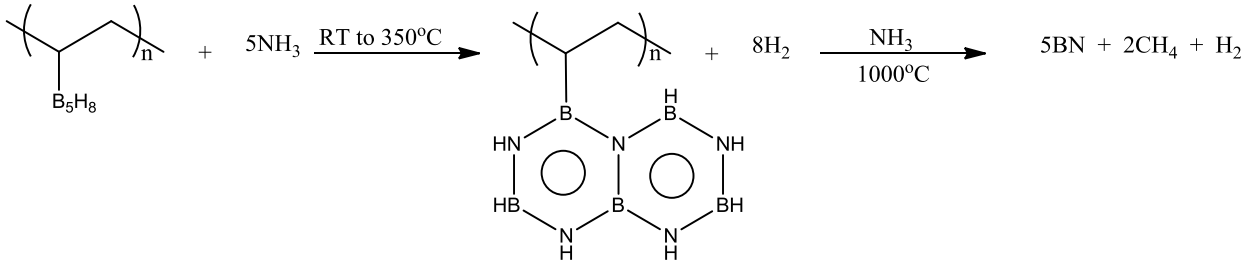

Scheme 4.1[10]- Schematic of poly(vinylpentaborane) pyrolyzed to 350°C under a ammonia gas to create a borazanaphthalene intermediate before producing BN.

With the presence of carbon in many of the polymer-based routes to BN, the distinct possibility of forming boron carbonitride (BCN) exists. BCN in its cubic configuration, has shown to have combined properties similar to diamond and cubic BN.[101] This relatively new branch of

superhard materials can achieve high melting temperatures, bulk modulus and thermal expansion coefficients similar to the high thermal and chemical stability of diamond.[102] The hexagonal structures can adapt to different compositions where they can behave as semiconductors with various band gap energies.[101]

There are various techniques in which boron carbonitride can be synthesized. In the early stages of research on this material, pure carbon and BN were heated to high temperatures.[103] Unfortunately, this method proved to have little success since phase separation prevented the actual bond hybridization of both the pure carbon and BN.[103] Advance techniques were created for gas phase reactions using chemical vapor deposition techniques, solid-phases pyrolysis, nitriding of solid phase precursors, solvothermal techniques, and polymeric precursors.[104] The majority of the polymeric preceramic precursors from these materials have been derived from borazine and borazine derivatives. Sneddon *et al.* were the first to report the pyrolysis of poly(vinylborazine), prepared via $RhH(CO)(PPh_3)_3$- catalyzed reaction of borazine with acetylene, under argon atmosphere.[105] Polymeric precursors that incorporated decaboranyl moieties pyrolyzed under nitrogen atmosphere to result in BCN have been reported.[8]

In this chapter, preliminary results of the pyrolysis of $p(NBE)_{60}$-*b*-$p(NDB)_{40}$ block copolymer discussed in chapter 3 were pyrolyzed under nitrogen atmosphere or ammonia gas to produce in BCN and BN ceramics.

Results and Discussion

Both BN and BCN were synthesized using the diblock copolymer p(NBE)$_{60}$-*b*-p(NDB)$_{40}$ that was previously discussed in Chapter 3. The process involved casting a film of the polymer in solution, evaporation of solvent and pyrolysis of the thin film of polymer purged with ammonia gas in a tube furnace to make BN ceramics. An analogous process was followed for BCN with exception of the purged ammonia gas during the heating cycle. The preparation of the thin films began with dissolving the p(NBE)$_{60}$-*b*-p(NDB)$_{40}$ into various dry solvents to make a 1mg/mL solution. The polymer was soluble in chloroform, DCM, toluene and THF but not in benzene or hexanes. It was observed that as the block copolymer ages under inert atmosphere for prolong periods of time, more time was required for the polymer to fully dissolve in solution. The solution was poured into a Teflon evaporating dish and slowly evaporated under inert atmosphere at RT. The slow evaporating rate allows the polymer to form the morphology structures.

The light orange/yellow casted thin film was transferred to a tube furnace. Prior to heating, the tube was sealed and purged with ammonia gas for 30 minutes to eliminate air in the system and reduce oxygen contamination. The heating cycles applied began with a ramp from RT at 5^{o}C/min to 400^{o}C, the sample was held at 400°C for one hour with a steady flow of ammonia gas. This was necessary to ensure crosslinking of BN and decomposition of the p(NBE) backbone. Sneddon *et al.* followed a similar procedure where poly(vinylpentaborane) was pyrolyzed with ammonia gas to produce borazine polymer intermediate (Scheme 4.1).[10] After dwelling at 400^{o}C, the samples were heated to 1000^{o}C with a 1°C/min ramp and held at

this temperature for 4 hours before cooling down to RT. The final BN product was a brittle black shiny solid with a ceramic yield of 53% with the theoretical yield of 60%.[8] The boron carbonitride product was a shiny dark grey and black solid with a ceramic yield of 56%.

Energy-dispersive x-ray spectroscopy (EDS) and elemental analysis (EA) were conducted to determine the atomic percent of the different elements present in the ceramics. The ceramics pyrolyzed under ammonia gas revealed an average of 38.84% of boron, 38.39% of nitrogen, 22.77% of oxygen with 7.24% of carbon and 1.34% of hydrogen revealed by EA (Figure 4.2). A 1:1 ratio of boron : nitrogen indicates that BN was produced with trace amounts of carbon and hydrogen retention accompanied by oxygen contamination from surface absorption[101]. Alternately, the ceramics produced under nitrogen gas, an average of 11.06% of boron, 11.34% of nitrogen, 12.12% of oxygen, 51.17% of carbon and 0.40% of hydrogen (Figure 4.3). A ratio of 5.62: 1.00: 1.02 of C: B: N reveals that there is an excess of carbon present in the ceramic that could be incorporated into different forms with boron and nitrogen. The possibility of $C_{5.62}B_{1.00}N_{1.02}$, carbon networks with BN domains; or BC_2N domains may all be present in the ceramic.

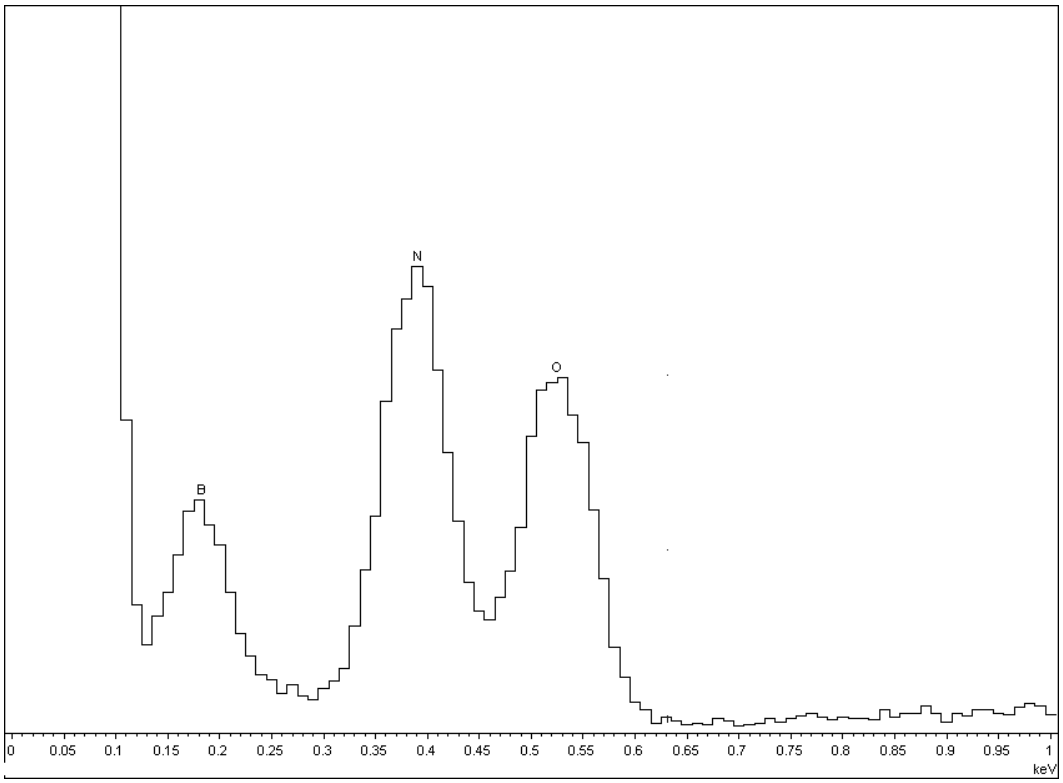

Figure 4.2- EDS of the BN ceramic from p(NBE)$_{60}$-*b*-p(NDB)$_{40}$ polymer pyrolyzed under ammonia gas at 1000^{o}C. Boron (38.84%), nitrogen (38.39%), and oxygen (22.77%) were detected.

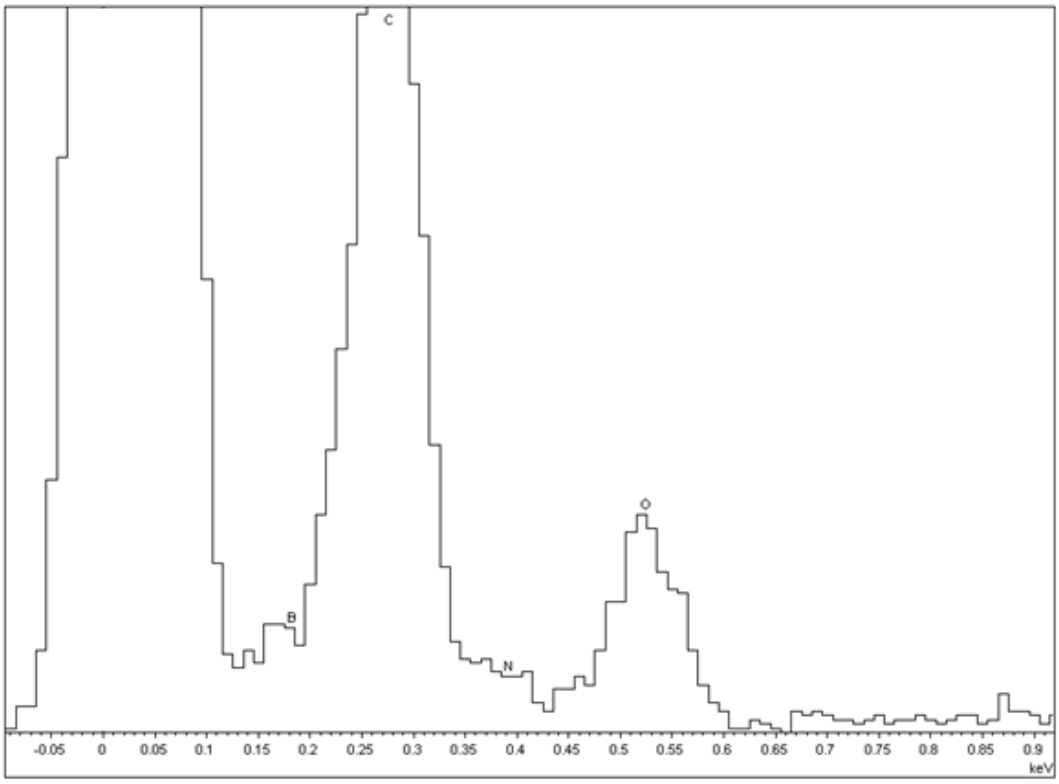

Figure 4.3- EDS of the BCN ceramic from p(NBE)$_{60}$-*b*-p(NDB)$_{40}$ polymer pyrolyzed under nitrogen gas at 1000^{o}C. Carbon (51.17%), boron (11.06%), nitrogen (11.34%), and oxygen (12.12%) were detected.

The SEM images of the ceramic products display the same morphologies as the cast thin film polymer SEMs (Figure 3.5). The p(NBE)$_{60}$-p(NDB)$_{40}$ polymer evaporated from chloroform than pyrolyzed under ammonia or nitrogen depicted more dense lamellar morphology since more material available to be analyzed (Figure 4.4 A). Several regions appear to have clusters of cylindrical-like morphologies as well that can be described as lamellar rotated by 90^{o} (Figure 4.4 B). There are regions that contain uniformly straight lines where the light line represent the BN matrix and the dark lines represent the void formerly occupied by carbon backbone. Higher

magnification images of these ceramics proved to be a challenge owing to the sample charging that occurred causing poor focus and permanent damage of the sample. The ceramic sample previously evaporated in THF, retained the disordered morphologies as seen in the copolymer SEM images (Figure 4.5). It contained random micelles were formed throughout the ceramic within the lamellar structure. This shows that self-assembly is formed via slow solvent evaporation and not particularly in the melt.

A)

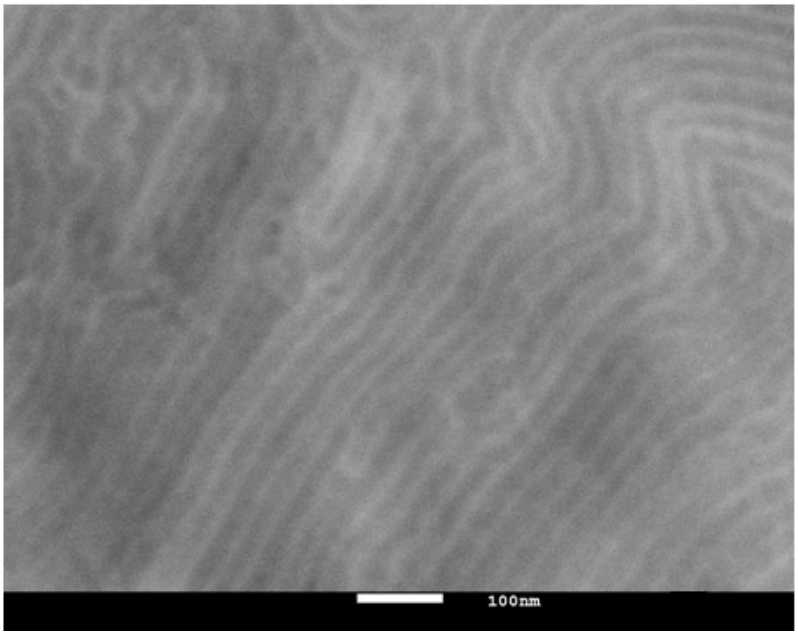

B)

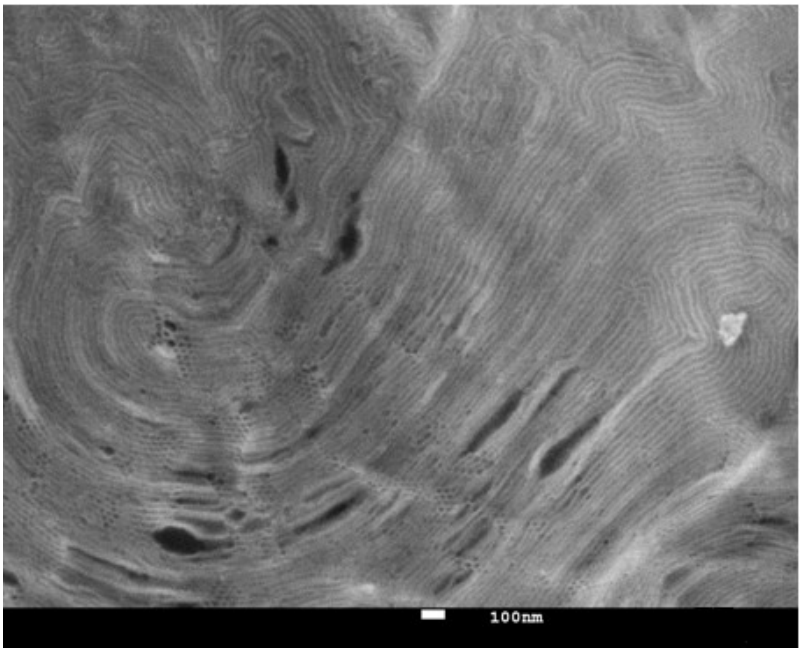

Figure 4.4- SEM images of $p(NBE)_{60}$-$p(NDB)_{40}$ polymer evaporated from chloroform than pyrolyzed under ammonia gas creating lamellar morphology patterns.

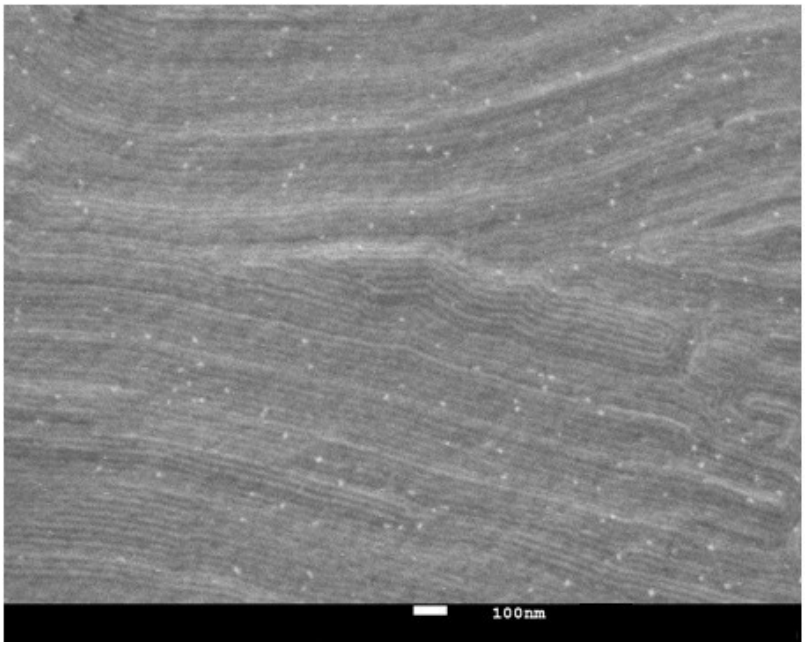

Figure 4.5- SEM images of $p(NBE)_{60}$-$p(NDB)_{40}$ polymer evaporated from THF than pyrolyzed under nitrogen gas.

The XRD analysis performed in these samples revealed a broad peak between 20^{o} to 30^{o} 2θ representative of an amorphous BN peak. No other significant peaks on the spectra were observed. As pyrolysis temperature reaching 1400^{o}C, BN is at a high purity and a sharp peak is shown between 23-30^{o} 2θ.[8] SAXS analysis on these ceramic did not reveal any extra information about the morphologies pattern with broad peaks caused by the nonuniform spacings between the blocks in the lamellar structures.

Experimental

The $p(NBE)_{60}$-$p(NDB)_{40}$ (0.400-0.450g) were dissolved in dry chloroform or tetrahydrofuran (1mg/mL) and transferred to a Teflon evaporating dish. The solution was allowed to slowly evaporate under inert atmosphere to produce a thin light yellow/light orange film. The films were carefully scraped off the dish and placed in boron nitride holding boats. The films were pyrolyzed under a steady flow of nitrogen or ammonia gas with a ramp cycle of 5^{o}C/min to 400^{o}C and dwelled for 1 hour. Continuing with a ramp cycle 1^{o}C/min to 1000^{o}C and dwelled for 4 hours then allowed to cool to RT.

Conclusion and Future Directions

The bis(mercapto) carboranes derivatives were successfully synthesized by a simple butyllithium reaction. The synthesis of the tethered cyano group requires more modifications to properly isolate the pure product. More investigations and advancement with these carboranes derivatives could not be continued because the chemical company ceased production of the carborane starting material for two years. In the future, adding other Raman-active functional group tethered to the *para*-carborane such as alkyne group should also be investigated for bioimaging.

Organic-organodecaborane diblock copolymers of p(NBE)-*b*-p(NDB) and p(NDC)-*b*-p(NDB) were synthesized and their self-assembly behaviour were analyzed. Different compositions of the block copolymer were analyzed and $p(NBE)_{60}$-*b*-$p(NDB)_{40}$ showed lamellar morphology patterns in chloroform. This diblock polymer was pyrolyzed to 1000^{o}C to make boron nitride and boron carbonitride ceramics and retained the same morphology patterns.

The boron nitride ceramics showed to have a small carbon contamination that could be eliminated if pyrolyzed to approximately 1400^{O}C. A larger family of these organic-organodecaborane block copolymers could be synthesized in the future to form all the possible morphological patterns. These could be pyrolyzed non-template boron nitride and boron carbonitride ceramics. Ceramic chemical and physical properties could be investigated by applying various ramp cycles during the pyrolysis process. These ceramics would have the potential to be utilized by applications such as catalysis, electrochemistry, and much more.

Appendix

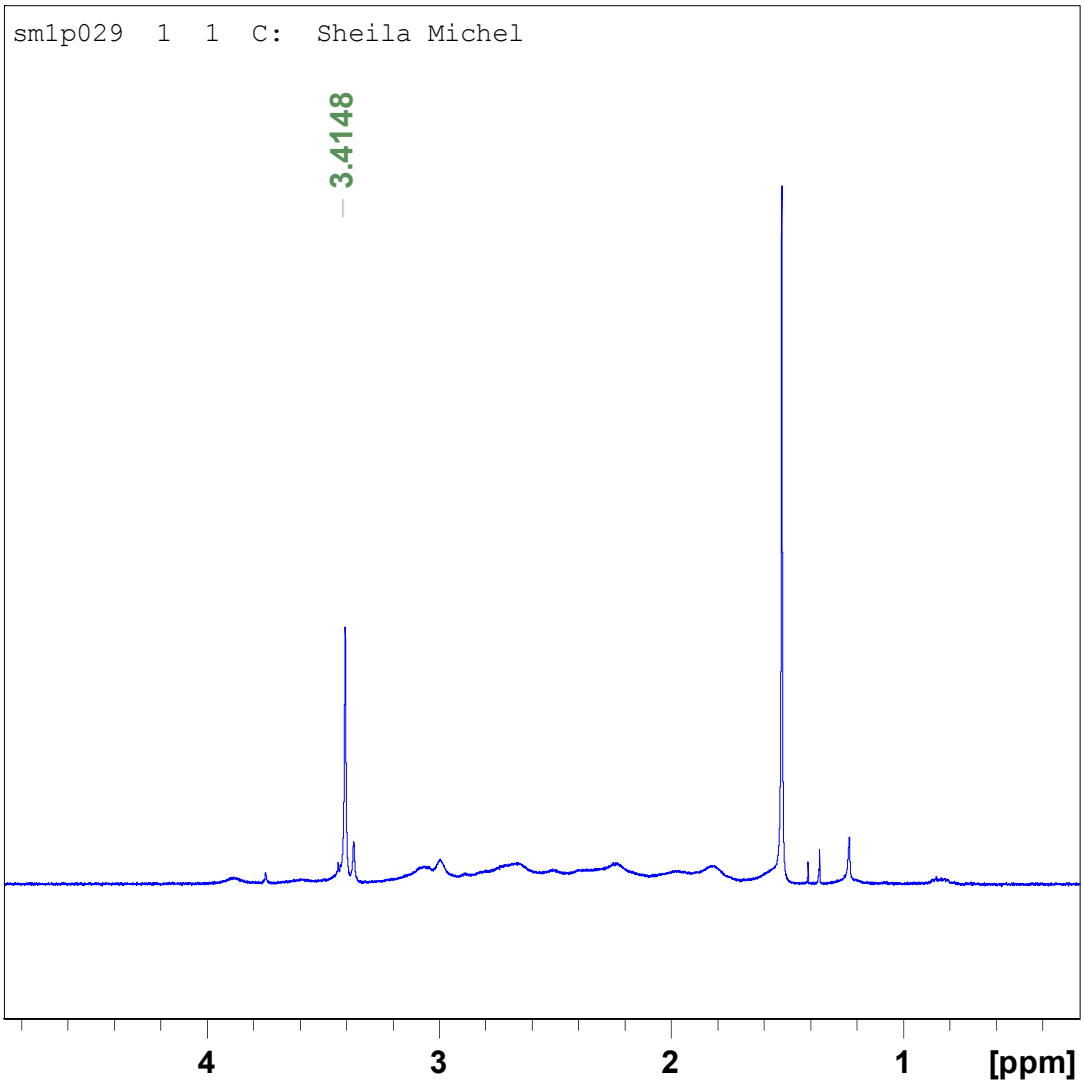

Figure A1. ^{1}H NMR (400 MHz, $CDCl_3$) of 1,7-bis(mercapto)-*m*-carborane.

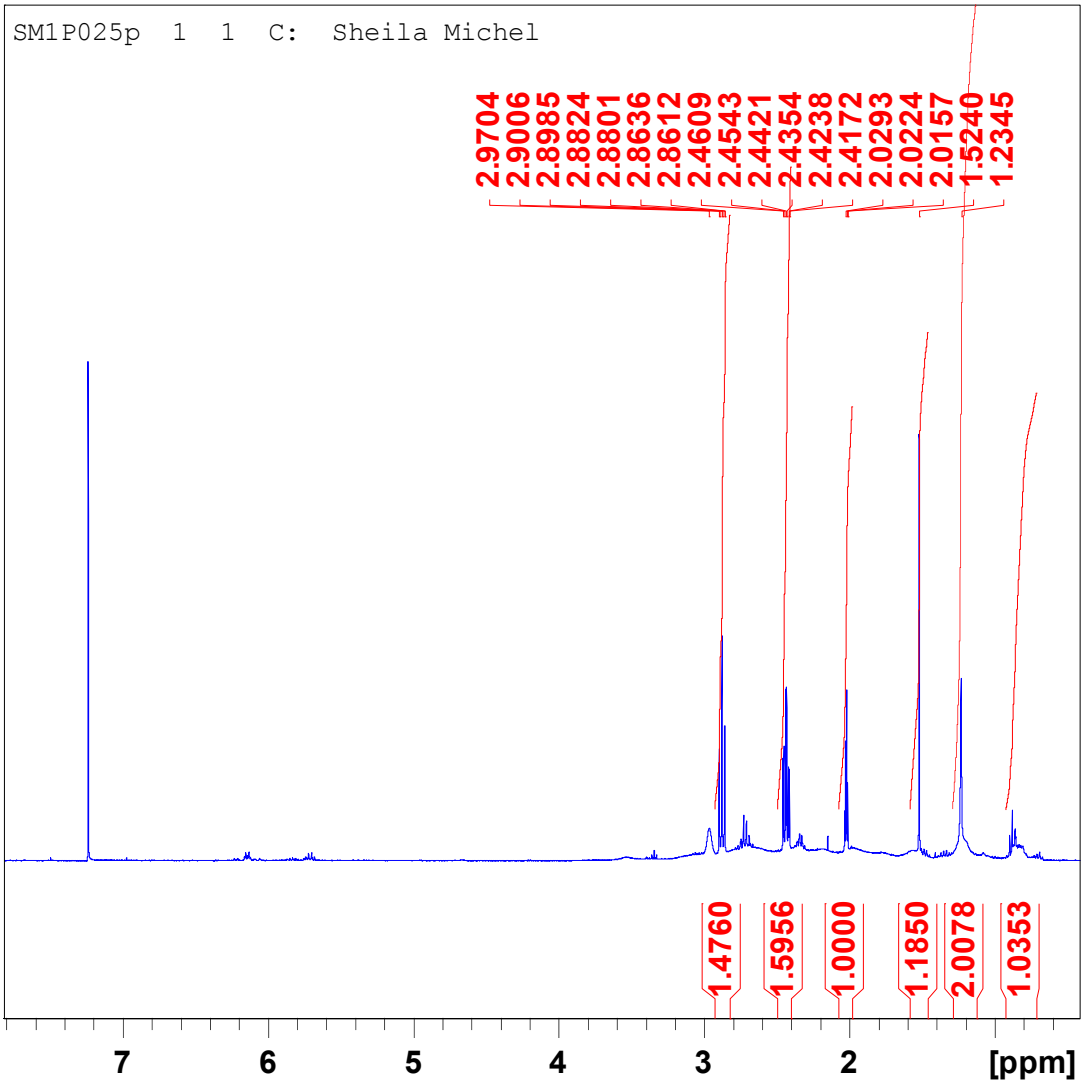

Figure A2. ^{1}H NMR (400 MHz, $CDCl_3$) of the crude product containing 1-(1-thio-propionitrile)-7-mercapto-*m*-carborane.

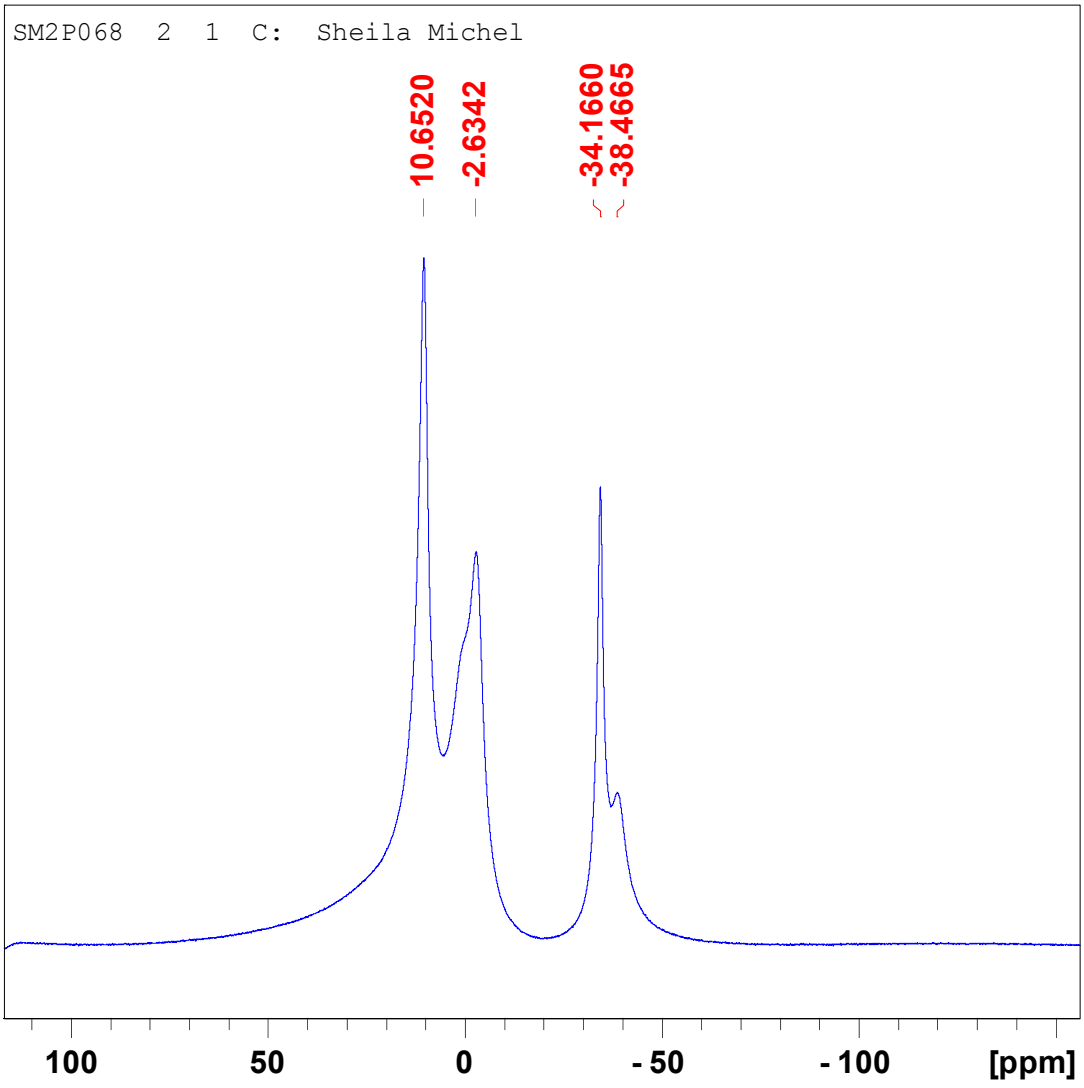

Figure A3. $^{11}B[^{1}H]$ NMR (300 MHz, $CDCl_3$) of $p(NBE)_{60}$-*b*-$p(NDB)_{40}$.

References

[1] R. W. Rudolph, *Accounts of Chemical Research* **1976**, *9*, 446.
[2] G. Kickelbick, U. Schubert, *Monatshefte Fur Chemie* **2001**, *132*, 13.
[3] F. S. F. Bates, G.H, *Physics Today* **1999**, *52*, 32.
[4] J. Grebenkemper*, Vol. 2012*, UC Davis ChemWiki by University of California, **2010**.
[5] A. Barron, in *Physical Methods in Inorganic and Nano Chemistry*, **2010**.
[6] D. C. Kennedy, D. R. Duguay, L. L. Tay, D. S. Richeson, J. P. Pezacki, *Chemical Communications* **2009**, 6750.
[7] T. Yamamoto, K. Nakai, A. Matsumura, *Cancer Letters* **2008**, *262*, 143.
[8] P. R. L. Malenfant, J. L. Wan, S. T. Taylor, M. Manoharan, *Nature Nanotechnology* **2007**, *2*, 43.
[9] T. U. o. Waikato, **2010**.
[10] M. G. L. Mirabelli, L. G. Sneddon, *Journal of the American Chemical Society* **1988**, *110*, 3305.
[11] a)X. Zhang, B. C. Berry, K. G. Yager, S. Kim, R. L. Jones, S. Satija, D. L. Pickel, J. F. Douglas, A. Karim, *ACS Nano* **2008**, *2*, 2331; b)Y. F. Shi, Y. Wan, R. Y. Zhang, D. Y. Zhao, *Advanced Functional Materials* **2008**, *18*, 2436.
[12] G. L. Miessler, *Inorganic chemistry*, 3rd ed., Pearson Prentice Hall, **2004**.
[13] V. I. Bregadze, *Chemical Reviews* **1992**, *92*, 209.
[14] E. D. Jemmis, E. G. Jayasree, *Accounts of Chemical Research* **2003**, *36*, 816.
[15] Wade, in *Advances in Inorganic Chemistry and Radiochemistry Serial Publication Series*, Academic Press, **1976**.
[16] M. N. Driess, H., *Molecular Clusters of the Main Group Elements*, John Wiley & Sons, **2008**.
[17] R. N. Grimes, *Carboranes*, 2nd ed., Academic press, **2011**.
[18] R. E. Williams, *Chemical Reviews* **1992**, *92*, 177.
[19] J. F. Valliant, K. J. Guenther, A. S. King, P. Morel, P. Schaffer, O. O. Sogbein, K. A. Stephenson, *Coordination Chemistry Reviews* **2002**, *232*, 173.
[20] S. Korbe, P. J. Schreiber, J. Michl, *Chemical Reviews* **2006**, *106*, 5208.
[21] C. M. Chung, S. J. Lee, J. G. Kim, D. O. Jang, *Journal of Non-Crystalline Solids* **2002**, *311*, 195.
[22] Y. Kwon, K. H. Kim, *Macromolecular Research* **2006**, *14*, 424.
[23] S. Kanaoka, R. H. Grubbs, *Macromolecules* **1995**, *28*, 4707.
[24] W. T. Xu, C. H. Chung, Y. W. Kwon, *Polymer* **2007**, *48*, 6286.
[25] D. B. Cordes, P. D. Lickiss, F. Rataboul, *Chemical Reviews* **2010**, *110*, 2081.
[26] A. V. Ruzette, L. Leibler, *Nature Materials* **2005**, *4*, 19.
[27] M. W. Matsen, M. Schick, *Physical Review Letters* **1994**, *72*, 2660.
[28] T. L. Morkved, H. M. Jaeger, *Europhysics Letters* **1997**, *40*, 643.

[29] Z. K. Z. Wang, W., *Scanning Microscopy for Nanotechnology- Techniques and Applications*, Springer, New York, **2006**.
[30] G. J. Exarhos, *Characterization of Optical Materials*, Momentum press, New York, **2010**.
[31] A. R. E. Clarke, C.N., *Microscopy Techniques for Materials Science*, Woodhead Publishing, New York, Washington D.C., Boston, **2002**.
[32] W. M. Groenewoud, *Characterisation of Polymers by Thermal Analysis*, Elsevier B.V., Netherlands, **2001**.
[33] E. Wilhelm, *Heat Capacities: Liquids, Solutions and Vapours*, Royal Society of Chemistry, **2010**.
[34] J. D. P. Menczel, R, Bruce *Thermal analysis of polymers : fundamentals and applications*, John Wiley, Hoboken, **2009**.
[35] S. R. K. Sandler, W. ; Bonesteel, J.; and Pearce, E.M., *Polymer Synthesis and Characterization :A Laboratory Manual*, Elsevier Inc, **1998**.
[36] R. C. Mackenzie, *International Union of Pure and Applied Chemistry* **1985**, *57*, 1737.
[37] Z. Grubisic, P. Rempp, H. Benoit, *Journal of Polymer Science Part B-Polymer Letters* **1967**, *5*, 753.
[38] B. G. Belen'kiĭ, Vilenchik, L.Z., *Modern Liquid Chromatography of Macromolecules, Volume 25*, Elsevier, **1983**.
[39] J. M. Sebastian, R. A. Register, *Journal of Applied Polymer Science* **2001**, *82*, 2056.
[40] T. Dumelow, S. R. Holding, L. J. Maisey, J. V. Dawkins, *Polymer* **1986**, *27*, 1170.
[41] B. Trathnigg, *Progress in Polymer Science* **1995**, *20*, 615.
[42] C. G. Pope, *Journal of Chemical Education* **1997**, *74*, 129.
[43] V. K. Z. Pecharsky, P.Y., *Fundamentals of Powder Diffraction and Structural Characterization of Materials*, 2nd ed. ed., Springer, Boston, **2009**.
[44] E. D. Smith, G., *Modern Raman Spectroscopy : A Practical Approach*, Wiley Hoboken, NJ, USA, **2005**.
[45] J. Kneipp, H. Kneipp, K. Kneipp, *Chemical Society Reviews* **2008**, *37*, 1052.
[46] S. Schlücker, *Surface Enhanced Raman Spectroscopy*, John Wiley & Sons, **2011**.
[47] E. C. E. Le Ru, P.G., *Principles of Surface-Enhanced Raman Spectroscopy: And Related Plasmonic Effects*, Elsevier, **2008**.
[48] M. Xiao, J. Nyagilo, V. Arora, P. Kulkarni, D. S. Xu, X. K. Sun, D. P. Dave, *Nanotechnology* **2010**, *21*.
[49] Y. Š. Ozaki, S., *Raman, infrared, and near-infrared chemical imaging* Wiley, Hoboken, **2010**.
[50] J. M. Nam, C. S. Thaxton, C. A. Mirkin, *Science* **2003**, *301*, 1884.
[51] M. Quinten, *Optical Properties of Nanoparticle Systems : Mie and Beyond*, John Wiley & Sons, Hoboken, **2011**.
[52] A. Campion, P. Kambhampati, *Chemical Society Reviews* **1998**, *27*, 241.
[53] M. A. Baia, S. ; Iliescu.t, *Raman and Sers Investigations of Pharmaceuticals*, Springer, **2008**.
[54] J. Bragin, D. S. Urevig, M. Diem, *Journal of Raman Spectroscopy* **1982**, *12*, 86.
[55] L. L. Yang, H. Mao, Y. A. Wang, Z. H. Cao, X. H. Peng, X. X. Wang, H. W. Duan, C. C. Ni, Q. G. Yuan, G. Adams, M. Q. Smith, W. C. Wood, X. H. Gao, S. M. Nie, *Small* **2009**, *5*, 235.
[56] J. V. Jokerst, T. Lobovkina, R. N. Zare, S. S. Gambhir, *Nanomedicine* **2011**, *6*, 715.

[57] A. H. Soloway, W. Tjarks, B. A. Barnum, F. G. Rong, R. F. Barth, I. M. Codogni, J. G. Wilson, *Chemical Reviews* **1998**, *98*, 2389.
[58] H. Joensuu, L. Kankaanranta, T. Seppala, I. Auterinen, M. Kallio, M. Kulvik, J. Laakso, J. Vahatalo, M. Kortesniemi, P. Kotiluoto, T. Seren, J. Karila, A. Brander, E. Jarviluoma, P. Ryynanen, A. Paetau, I. Ruokonen, H. Minn, M. Tenhunen, J. Jaakelainen, M. Farkkila, S. Savolainen, *Journal of Neuro-Oncology* **2003**, *62*, 123.
[59] A. K. A. A. Azab, H. ; Srebnik, M. , in *Studies in Inorganic Chemistry, Vol. 22*, Elsevier, **2007**, pp. 337.
[60] M. M. Amiji, *Nanotechnology for Cancer Therapy*, CRC Press, **2007**.
[61] R. F. Barth, W. L. Yang, A. S. Al-Madhoun, J. Johnsamuel, Y. Byun, S. Chandra, D. R. Smith, W. Tjarks, S. Eriksson, *Cancer Research* **2004**, *64*, 6287.
[62] E. I. Tolpin, G. R. Wellum, F. C. Dohan, P. L. Kornblith, R. G. Zamenhof, *Oncology* **1975**, *32*, 223.
[63] A. H. Soloway, H. Hatanaka, M. A. Davis, *Journal of Medicinal Chemistry* **1967**, *10*, 714.
[64] D. Slatkin, P. Micca, A. Forman, D. Gabel, L. Wielopolski, R. Fairchild, *Biochemical Pharmacology* **1986**, *35*, 1771.
[65] B. T. S. Thirumamagal, X. B. Zhao, A. K. Bandyopadhyaya, S. Narayanasamy, J. Johnsamuel, R. Tiwari, D. W. Golightly, V. Patel, B. T. Jehning, M. V. Backer, R. F. Barth, R. J. Lee, J. M. Backer, W. Tjarks, *Bioconjugate Chemistry* **2006**, *17*, 1141.
[66] X. H. Huang, I. H. El-Sayed, W. Qian, M. A. El-Sayed, *Nano Letters* **2007**, *7*, 1591.
[67] I. H. El-Sayed, X. H. Huang, M. A. El-Sayed, *Cancer Letters* **2006**, *239*, 129.
[68] T. P. Lodge, *Macromolecular Chemistry and Physics* **2003**, *204*, 265.
[69] T. M. Trnka, R. H. Grubbs, *Accounts of Chemical Research* **2001**, *34*, 18.
[70] T. L. Choi, R. H. Grubbs, *Angewandte Chemie-International Edition* **2003**, *42*, 1743.
[71] G. O. Wilson, K. A. Porter, H. Weissman, S. R. White, N. R. Sottos, J. S. Moore, *Advanced Synthesis & Catalysis* **2009**, *351*, 1817.
[72] a)S. D. Drouin, G. P. A. Yap, D. E. Fogg, *Inorganic Chemistry* **2000**, *39*, 5412; b)S. D. Drouin, F. Zamanian, D. E. Fogg, *Organometallics* **2001**, *20*, 5495.
[73] J. K. Huang, H. J. Schanz, E. D. Stevens, S. P. Nolan, *Organometallics* **1999**, *18*, 5375.
[74] M. S. Sanford, J. A. Love, R. H. Grubbs, *Journal of the American Chemical Society* **2001**, *123*, 6543.
[75] T. Weskamp, F. J. Kohl, W. A. Herrmann, *Journal of Organometallic Chemistry* **1999**, *582*, 362.
[76] C. W. Bielawski, R. H. Grubbs, *Angewandte Chemie-International Edition* **2000**, *39*, 2903.
[77] R. H. Grubbs, *Tetrahedron* **2004**, *60*, 7117.
[78] J. A. Love, J. P. Morgan, T. M. Trnka, R. H. Grubbs, *Angewandte Chemie-International Edition* **2002**, *41*, 4035.
[79] J. A. Love, M. S. Sanford, J. P. Morgan, R. H. Grubbs, *Abstracts of Papers of the American Chemical Society* **2002**, *224*, U153.
[80] S. Sutthasupa, M. Shiotsuki, H. Matsuoka, T. Masuda, F. Sanda, *Macromolecules* **2010**, *43*, 1815.
[81] a)S. Karabulut, V. Sahin, B. O. Ozturk, Y. Imamoglu, *Journal of Inorganic and Organometallic Polymers and Materials* **2009**, *19*, 570; b)T. S. Haddad, P. T. Mather, H.

G. Jeon, A. Romo-Uribe, A. R. Farris, J. D. Lichtenhan, *Organic/Inorganic Hybrid Materials* **1998**, *519*, 381.
[82] X. L. Wei, P. J. Carroll, L. G. Sneddon, *Chemistry of Materials* **2006**, *18*, 1113.
[83] J. F. Hartwig, C. N. Muhoro, *Organometallics* **2000**, *19*, 30.
[84] M. J. Pender, P. J. Carroll, L. G. Sneddon, *Journal of the American Chemical Society* **2001**, *123*, 12222.
[85] S. Hermanek, *Chemical Reviews* **1992**, *92*, U175.
[86] L. G. Sneddon, A. T. Lynch, J. S. Beck, W. Keller, M. G. L. Mirabelli, *Abstracts of Papers of the American Chemical Society* **1989**, *198*, 89.
[87] M. A. Esteruelas, F. Gonzalez, J. Herrero, P. Lucio, M. Olivan, B. Ruiz-Labrador, *Polymer Bulletin* **2007**, *58*, 923.
[88] a)M. Kamperman, C. B. W. Garcia, P. Du, H. S. Ow, U. Wiesner, *Journal of the American Chemical Society* **2004**, *126*, 14708; b)Y. Meng, D. Gu, F. Q. Zhang, Y. F. Shi, H. F. Yang, Z. Li, C. Z. Yu, B. Tu, D. Y. Zhao, *Angewandte Chemie-International Edition* **2005**, *44*, 7053; c)R. Ryoo, S. H. Joo, S. Jun, *Journal of Physical Chemistry B* **1999**, *103*, 7743.
[89] A. S. Lipp, K.A. ; Hunold, K., *Journal of the European Ceramic Society* **1989**, *5*, 3.
[90] P. Gleize, M. C. Schouler, P. Gadelle, M. Caillet, *Journal of Materials Science* **1994**, *29*, 1575.
[91] C. K. Narula, *Ceramic precursor technology and its applications*, M.Dekker, New York, **1995**.
[92] W. J. Zhang, X. M. Meng, C. Y. Chan, K. M. Chan, Y. Wu, I. Bello, S. T. Lee, *Journal of Physical Chemistry B* **2005**, *109*, 16005.
[93] J. Nocua, #233, E., F. Piazza, B. R. Weiner, G. Morell, *Journal of Nanomaterials* **2009**, *2009*.
[94] T. Sato, T. Ishii, N. Setaka, *Journal of the American Ceramic Society* **1982**, *65*, C162.
[95] R. Haubner, M. Wilhelm, R. Weissenbacher, B. Lux, *High Performance Non-Oxide Ceramics Ii* **2002**, *102*, 1.
[96] R. Arenal, X. Blase, A. Loiseau, *Advances in Physics* **2010**, *59*, 101.
[97] S. I. Hirano, T. Yogo, S. Asada, S. Naka, *Journal of the American Ceramic Society* **1989**, *72*, 66.
[98] M. G. L. Mirabelli, L. G. Sneddon, *Inorganic Chemistry* **1988**, *27*, 3271.
[99] T. Yogo, S. Matsuo, S. Naka, *Yogyo-Kyokai-Shi* **1987**, *95*, 94.
[100] W. S. Rees, D. Seyferth, *Journal of the American Ceramic Society* **1988**, *71*, C194.
[101] F. L. Huang, C. B. Cao, X. Xiang, R. T. Lv, H. S. Zhu, *Diamond and Related Materials* **2004**, *13*, 1757.
[102] K. Yuge, *Journal of Physics-Condensed Matter* **2009**, *21*.
[103] M. L. Kosinova, Y. M. Rumyantsev, N. I. Fainer, E. A. Maximovski, F. A. Kuznetsov, *Nuclear Instruments & Methods in Physics Research Section a-Accelerators Spectrometers Detectors and Associated Equipment* **2001**, *470*, 253.
[104] a)J. Yu, E. G. Wang, G. C. Xu, *Chemical Physics Letters* **1998**, *292*, 531; b)R. Riedel, J. Bill, G. Passing, *Advanced Materials* **1991**, *3*, 551.
[105] P. J. Fazen, E. E. Remsen, J. S. Beck, P. J. Carroll, A. R. Mcghie, L. G. Sneddon, *Chemistry of Materials* **1995**, *7*, 1942.